Journal of Medicinal Chemistry

pubs.acs.org/jmc

Article

Syntheses, Biological Evaluations, and Mechanistic Studies of Benzo[*c*][1,2,5]oxadiazole Derivatives as Potent PD-L1 Inhibitors with *In Vivo* Antitumor Activity

Liu Liu,[‖] Zhiying Yao,[‖] Shijun Wang,[‖] Tao Xie, Guoqing Wu, Honghan Zhang, Pu Zhang, Yaojun Wu, Haoliang Yuan,[*] and Hongbin Sun[*]

Cite This: *J. Med. Chem.* 2021, 64, 8391−8409

Read Online

ACCESS | Metrics & More | Article Recommendations | Supporting Information

ABSTRACT: A series of novel benzo[*c*][1,2,5]oxadiazole derivatives were designed, synthesized, and biologically evaluated as inhibitors of PD-L1. Among them, compound **L7** exhibited 1.8 nM IC_{50} value in a homogeneous time-resolved fluorescence (HTRF) assay, which was 20-fold more potent than the lead compound **BMS-1016**. In the surface plasmon resonance (SPR) assay, **L7** bound to human PD-L1 (hPD-L1) with a K_D value of 3.34 nM, without showing any binding to hPD-1. In the cell-based coculture assay, **L7** blocked PD-1/PD-L1 interaction with an EC_{50} value of 375 nM, while **BMS-1016** had an EC_{50} value of 2075 nM. Moreover, compound **L24**, an ester prodrug of **L7**, was orally bioavailable and displayed significant antitumor effects in tumor models of syngeneic and PD-L1 humanized mice. Mechanistically, **L24** exhibited significant *in vivo* antitumor effects probably through promoting antitumor immunity. Together, this series of benzoxadiazole PD-L1 inhibitors holds promise for tumor immunotherapy. Preclinical trials with selected compounds are ongoing in our laboratory.

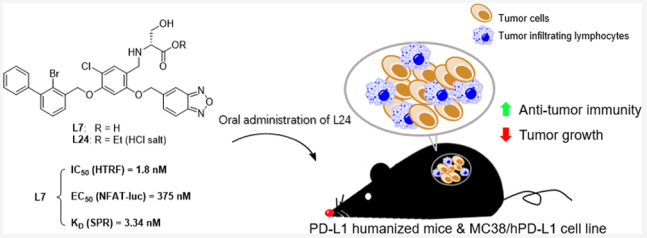

INTRODUCTION

In the past decade, cancer immunotherapy based on the blockade of immune checkpoints has made great strides.[1,2] In particular, monoclonal antibodies (mAbs) of programmed cell death protein 1 (PD-1) and programmed cell death-ligand 1 (PD-L1) have been very successful for the treatment of various tumors, including nonsmall cell lung cancer (NSCLC), urothelial cancer, melanoma, head and neck squamous cell cancer, and lymphoma.[3−5] Recently, encouraging results from several phase III clinical trials showed that combinations of PD-1/PD-L1 antibodies and antiangiogenic agents are very effective for treating NSCLC (adenocarcinoma) and hepatocellular carcinoma.[6,7] Until now, there are six PD-1/PD-L1 antibodies (anti-PD-1, nivolumab, pembrolizumab, and cemiplimab; anti-PD-L1, atezolizumab, avelumab, and durvalumab) approved by the US Food and Drug Administration (FDA) for clinical applications.[8] Despite their broad applicability in cancer treatment, the shortcomings of PD-1/PD-L1 antibodies exist, such as low response rates with a range of 10−30% in most cancers, autoimmune symptoms, and tumor hyperprogression.[8,9] On the other hand, small-molecule inhibitors of the PD-1/PD-L1 protein−protein interaction have attracted much attention due to their absent or weak immunogenicity, improved tumor penetration, better oral bioavailability, manipulative immune-related adverse effects (irAEs), and low cost.[8,10]

Both PD-1 and PD-L1 are membrane proteins and interact with each other through their canonical immunoglobulin (Ig)-like extracellular domains, essentially via hydrophobic and polar interactions involving two front β-sheets and connecting loops.[11] Like most of the B7 protein family members, PD-L1 could form a homodimer in the solution or crystalline state, either in the presence or absence of its ligand.[11−13] Although the structural studies on the hPD-1/hPD-L1 complex pointed to the 1:1 stoichiometry, it cannot be ruled out the possibility that the PD-L1 homodimer binds to PD-1 since no steric hindrance seems to exist in this context.[13] By far, some nonpeptide small-molecule and peptidomimetic inhibitors of the PD-1/PD-L1 protein−protein interaction have been developed (Figure 1).[8,14−17] Bristol-Myers Squibb (BMS) has developed a series of biphenyl compounds including **BMS-202** (**1**)[18] and **BMS-1016** (**2**),[19] which are among the most potent lead compounds of PD-L1 inhibitors. Cocrystal structures of the complexes of PD-L1 bound to **BMS-202** and related compounds show that a single BMS compound binds to two PD-L1 protein molecules, indicating the formation of PD-L1 homodimers induced and stabilized by the small-molecule compounds.[10,11,20] PD-L1 inhibitors **3**/**4**/**5**

Received: March 4, 2021
Published: June 11, 2021

https://doi.org/10.1021/acs.jmedchem.1c00392
J. Med. Chem. 2021, 64, 8391−8409

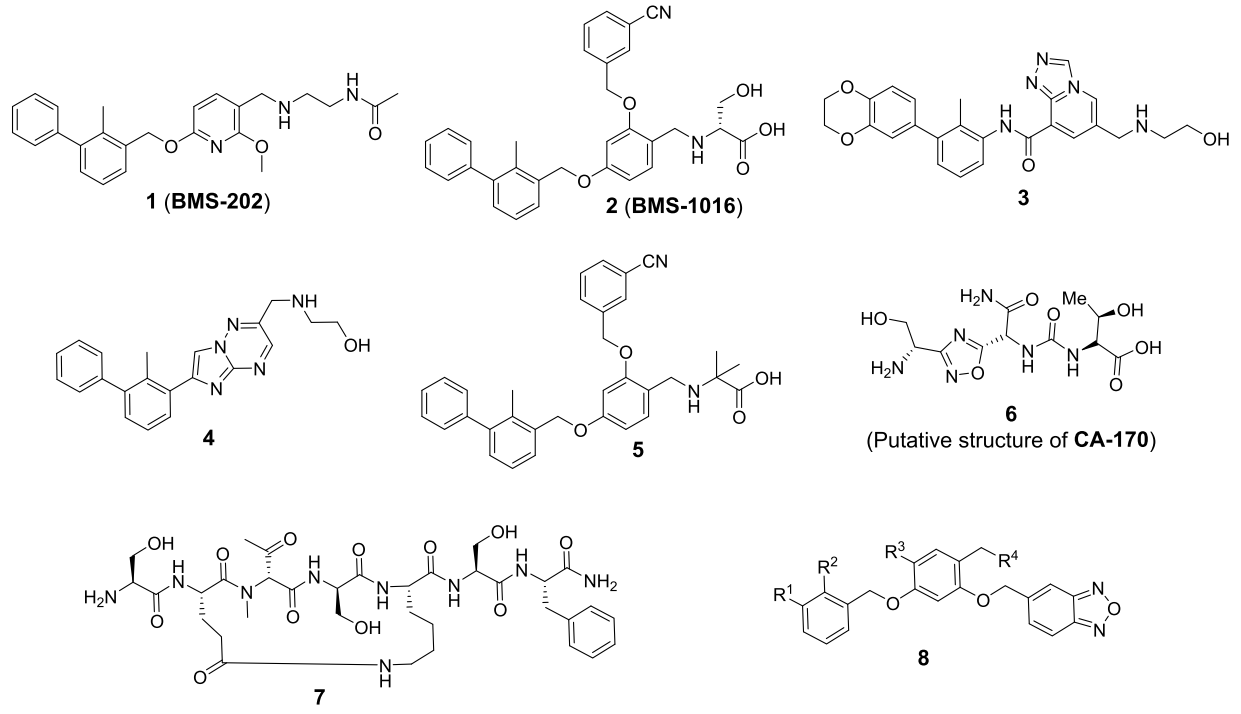

Figure 1. Chemical structures of small-molecule inhibitors of PD-1/PD-L1 interaction.

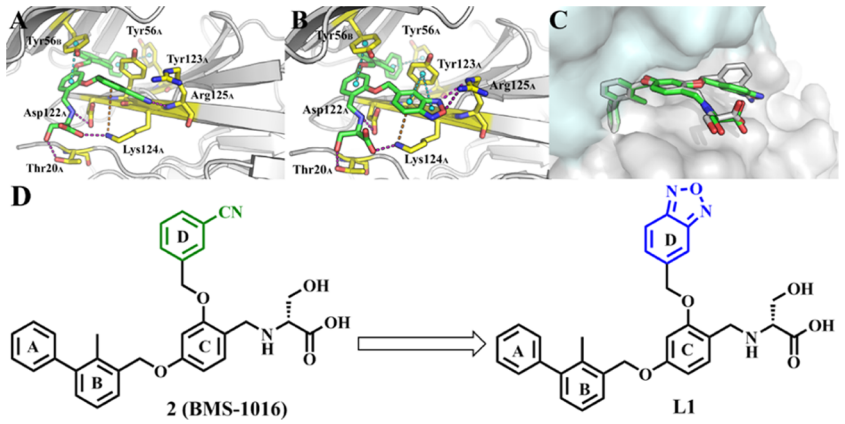

Figure 2. Binding modes of **BMS-1016** (A) and **L1** (B) in the pocket of the PD-L1 homodimer predicted by molecular docking. The $\pi-\pi$ stacking interactions were shown as a green dash line, $\pi-$cation interactions were shown as an orange dash line, and hydrogen-bonding interactions were shown as a magenta dash line. (C) Alignment of **BMS-1016** (gray) and **L1** (green) in the cleft formed by the PD-L1 dimer (the docking model was based on the dimeric PD-L1 protein taken from PDB ID: 5J89). (D) Design of benzo[*c*][1,2,5]oxadiazole small-molecule inhibitors of PD-1/PD-L1 protein−protein interaction.

were developed on the basis of BMS compounds. Peptidomimetic inhibitors **6**/**7** were developed by Curis and Aurigene. One of the most advanced small-molecule immune checkpoint inhibitors is the peptidomimetic compound **CA-170**, which is thought to be a dual inhibitor of PD-L1 and V-domain Ig suppressor of T-cell activation (VISTA). In a phase II clinical trial on multitumors, **CA-170** was well tolerated and showed clinical benefit across tumor types with an incidence of irAEs (https://www.curis.com/pipeline/ca-170/). Nevertheless, the results of a comprehensive characterization of small-molecule PD-L1 inhibitors demonstrated that **CA-170** had neither direct binding to PD-L1 nor interference on PD-1/PD-L1 interaction.[21] Other small-molecule PD-L1 inhibitors entering clinical trials include **INCB86550** (Incyte Corp.), **GS-4224** (Gilead), **MAX-10181** (MaxiNovel Pharma., China), etc.

The challenges of developing small-molecule PD-L1 inhibitors for clinical applications still exist, such as inadequate efficacy and specificity compared to mAbs, lack of mechanistic insight into their *in vivo* immunoactivation activity, and incomplete structural information for ligand recognition. In this study, a series of benzo[*c*][1,2,5]oxadiazole derivatives (**8**) based on the BMS scaffold were designed and synthesized as new PD-L1 inhibitors. The results of *in vitro* assays, including homogeneous time-resolved fluorescence (HTRF), surface plasmon resonance (SPR), coculture assay, identified compound **L7** as a potent PD-L1 inhibitor that blocked PD-1/PD-L1 interaction at both protein and cellular levels. An orally bioavailable prodrug of **L7** exhibited significant antitumor activity in tumor models of syngeneic and PD-L1 humanized mice. Mechanistically, this prodrug (**L24**) suppressed tumor

https://doi.org/10.1021/acs.jmedchem.1c00392
J. Med. Chem. 2021, 64, 8391−8409

growth likely through upregulating cytotoxic T and NK cells while downregulating immunosuppressive cells.

RESULTS AND DISCUSSION

Molecular Design. The cocrystal structure of **BMS-202** bound to PD-L1 (PDB ID: 5J89) reveals that the biphenyl moiety of **BMS-202** is located in a deep, cylindrical, hydrophobic pocket created by the interface of the dimeric PD-L1 protein to generate multiple hydrophobic interactions with surrounding amino acid residues.[20] Multiple experiments have proved that the biphenyl moiety is essential for the inhibitors to block the interaction of PD-1/PD-L1.[11] With using **BMS-1016** as a lead compound, we hoped to develop more potent PD-L1 inhibitors with new scaffolds. Molecular docking of **BMS-1016** to the PD-L1 homodimer revealed that $\pi-\pi$ stacking interactions were formed between ring A and $Tyr56_A$ and ring C and $Tyr56_B$ (Figure 2A). The hydrophilic D-serine moiety formed hydrogen-bonding interactions with adjacent residues $Thr20_A$, $Asp122_A$, and $Lys124_A$. Ring D occupied a pocket surrounded by $Tyr123_A$, $Lys124_A$, and $Arg125_A$. A single hydrogen bond was generated between the CN group of 3-cyanobenzyl substituent and $Arg125_A$, while π-cation interaction was found between ring D and $Lys124_A$ (Figure 2A). Of note, the pharmacophoric features of this pocket indicated that it was possible to find more potent PD-L1 inhibitors by replacing the 3-cyanobenzyl side chain with groups, forming additional protein−ligand interactions. Considering the aromatic property of the $Tyr123_A$ residue, along with the positive charged $Arg125_A$ and $Lys124_A$, we focused on using benzoheterocyclic groups as the alternative substituents to achieve stronger binding affinity with better binding mode. Several benzoheterocyclic compounds **L1**−**L4** (Table 1) were thus designed as close analogues of **BMS-1016**. Among them, benzoxadiazole compound **L1** showed well alignment of the binding mode with **BMS-1016** (Figure 2B,C). Importantly, the benzoxadiazole moiety showed additional $\pi-\pi$ stacking interaction with $Tyr123_A$ while keeping all of the other interactions. The Glide docking scores of **BMS-1016** and **L1** were −13.085 and −13.195 kcal/mol, respectively, indicating the good potential of **L1** as a novel lead compound of PD-L1 inhibitors.

Chemistry. Synthesis of compounds **L1**−**L4** is depicted in Scheme 1. Selective *O*-alkylation of 2,4-dihydroxybenzaldehyde with benzyl bromide **9** in the presence of $NaHCO_3$ in refluxing acetonitrile afforded phenol-aldehyde **10** in 83% yield. Further *O*-alkylation of **10** with benzoheterocyclic benzyl bromide in the presence of cesium carbonate gave aldehydes **11a**−**d** in 92−99% yields (see the Supporting Information, SI). Borch reductive amination of **11a**−**d** with D-serine ethyl ester in the presence of sodium triacetoxyborohydride followed by hydrolysis of the resulting esters provided the target compounds **L1**−**L4**.

In a similar pattern, compounds **L5**−**L12** and **L24**−**L42** were synthesized (Scheme 2). Therefore, dihydroxybenzaldehydes **X1**−**3** were selectively alkylated with benzylbromides (**9**, **12a**−**d**) to afford hydroxybenzaldehydes **13a**−**h**, which were further alkylated with 5-(bromomethyl)-2,1,3-benzoxadiazole to furnish aldehydes **14a**−**h** in 89−93% yields (see the SI). Reductive amination of **14a**−**h** with D-serine ethyl ester followed by hydrolysis of the resulting esters gave compounds **L5**−**L12**. Reductive amination of **14c** with D-serine ethyl ester furnished ester prodrug **L24**. Reductive amination of **14c** with L-serine ethyl ester furnished compound **L25** as an enantiomer of **L7**. Reductive amination of **14c** or **14d** with other amino acid esters followed by hydrolysis of the resulting esters gave compounds **L26**, **L28**, **L30**, **L37**, **L41**, and **L42**. Reductive amination of **14c** or **14d** with other amines afforded compounds **L27**, **L29**, **L31**−**36**, and **L38**−**40**.

Synthesis of compounds **L13**−**L23** is depicted in Scheme 3. Selective *O*-alkylation of 2,4-dihydroxy-5-chlorobenzaldehyde with 3-iodo-benzylbromides **15a**−**b** afforded phenol-aldehydes **16a**−**b** in 65−75% yields. The Suzuki−Miyaura coupling reaction between **16a**−**b** and phenylboronic acid derivatives provided biphenyl compounds **17a**−**k**. *O*-Alkylation of **17a**−**k** with 5-(bromomethyl)-2,1,3-benzoxadiazole gave benzoxadiazole compounds **18a**−**k** (see the SI). Reductive amination of **18a**−**k** with D-serine ethyl ester followed by hydrolysis of the resulting esters provided compounds **L13**−**L23** in 19−33 yields (two steps).

Table 1. PD-1/PD-L1 Blockade Effect of Benzoheterocycle Compounds L1−L4[a]

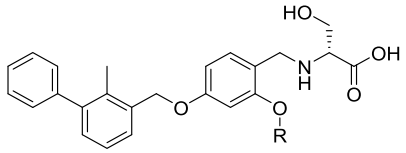

Compound	R	IC_{50} (nM) HTRF [a]
L1	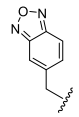	33.7±2.9
L2		2159.5±38.9
L3	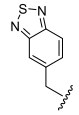	205.6±149.8
L4	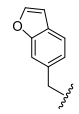	2343.5±374.1
BMS-1016		35.8±7.3

[a]The data were generated from two independent experiments.

HTRF Assay for PD-1/PD-L1 Blockade and Structure−Activity Relationship (SAR) Analysis. The blockade effect of the compounds on PD-1/PD-L1 interaction was examined by the HTRF assay. As shown in Table 1, benzoheterocyclic compounds **L1**−**L4** had substantially varying potency with IC_{50} values ranging from nanomoles to micromoles. Among them, **L1** with a benzo[*c*][1,2,5]oxadiazol-5-ylmethoxy moiety exhibited potency (IC_{50} = 33.7 nM) comparable to that of **BMS-1016** (IC_{50} = 35.8 nM). The potency of **L2** (IC_{50} = 2159.5 nM) with a benzo[*c*][1,2,5]oxadiazol-4-ylmethoxy moiety and **L4** (IC_{50} = 2343.5 nM) with a benzofuran-6-ylmethoxy moiety significantly decreased. **L3** (IC_{50} = 205.6

https://doi.org/10.1021/acs.jmedchem.1c00392
J. Med. Chem. 2021, 64, 8391−8409

Scheme 1. Synthesis of Compounds L1−L4[a]

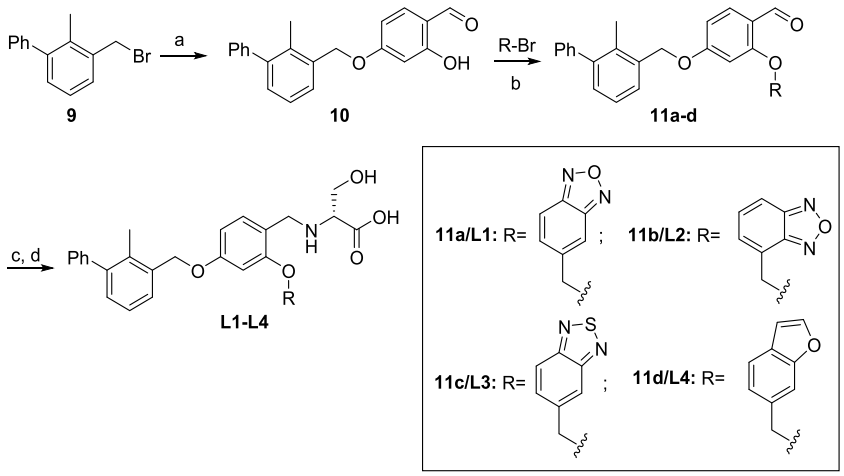

[a]Reagents and conditions: (a) 2,4-dihydroxybenzaldehyde, $NaHCO_3$, MeCN, reflux, 83%. (b) R-Br, Cs_2CO_3, *N*,*N*-dimethylformamide (DMF), rt, 92−99%. (c) D-Serine ethyl ester hydrochloride, $NaBH(OAc)_3$, *N*,*N*-diisopropylethylamine (DIPEA), dichloromethane (DCM), AcOH, rt. (d) LiOH, MeOH, rt, then neutralized by 1 N HCl, two steps, 13−26%.

Scheme 2. Synthesis of Compounds L5−L12 and L24−L42[a]

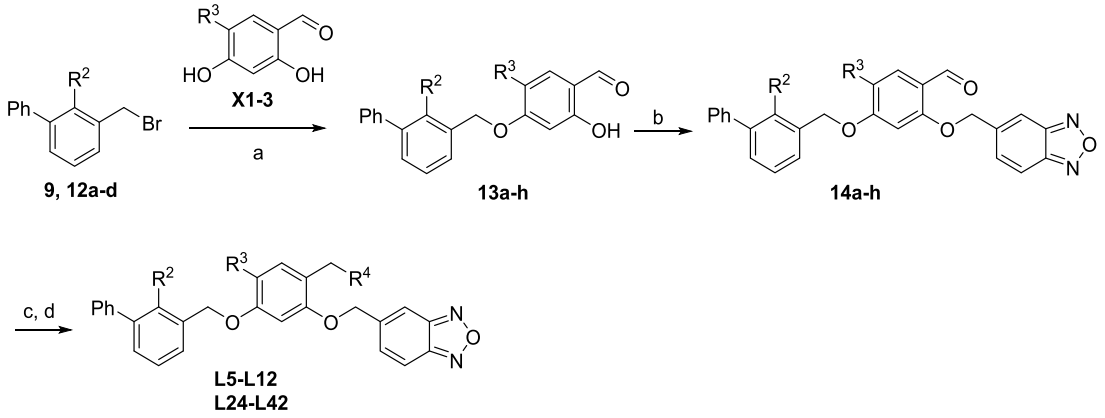

[a]Reagents and conditions: (a) $NaHCO_3$, MeCN, reflux, 63−82%. (b) 5-(Bromomethyl)-2,1,3-benzoxadiazole, Cs_2CO_3, DMF, rt, 89−93%. (c) D-Serine ethyl ester hydrochloride or other amines, $NaBH(OAc)_3$, DCM, AcOH, rt, 19−30%. (d) In case amino acid esters were used for the reductive amination reaction, hydrolysis of the resulting esters was performed using the following conditions: LiOH, MeOH, rt, then neutralized by 1 N HCl.

Scheme 3. Synthesis of Compounds L13−L23[a]

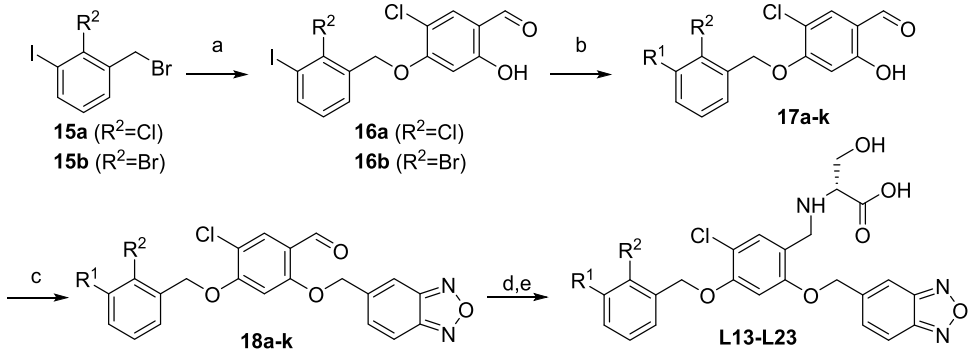

[a]Reagents and conditions: (a) 2,4-dihydroxy-5-chlorobenzaldehyde, $NaHCO_3$, MeCN, reflux, 65−75%. (b) Phenylboronic acid derivatives, $Pd(dppf)Cl_2{\cdot}CH_2Cl_2$, K_2CO_3, PhMe, EtOH, H_2O, reflux, 40−48%. (c) 5-(Bromomethyl)-2,1,3-benzoxadiazole, Cs_2CO_3, DMF, rt, 82−90%. (d) D-Serine ethyl ester hydrochloride, $NaBH(OAc)_3$, DIPEA, DCM, AcOH, rt. (e) LiOH, MeOH, rt, then neutralized by 1 N HCl, two steps, 19−33%.

nM) with a benzo[*c*][1,2,5]thiadiazol-5-ylmethoxy moiety was sixfold less potent than **L1**. Together, the benzo[*c*][1,2,5]-oxadiazol-5-ylmethoxy unit of **L1** was proved to be a privileged scaffold for the design of new PD-1/PD-L1 inhibitors.

https://doi.org/10.1021/acs.jmedchem.1c00392
J. Med. Chem. 2021, 64, 8391−8409

With **L1** as a novel lead compound, structural modifications on the biphenyl unit (B ring) and the central benzene ring (C ring) were conducted to provide compounds **L5**–**L12** (Table 2). HTRF assay results showed that replacement of the methyl group of **L1** with trifluoromethyl group caused a sharp decrease in potency (**L5**: IC_{50} = 1384.5 nM). Introduction of 5-Cl substitution at the central benzene ring of **L1** led to increased potency (**L6**: IC_{50} = 16.6 nM). Notably, replacement of the methyl group of **L6** with bromine, chlorine, or fluorine caused significantly improved potency (**L7**: IC_{50} = 1.8 nM; **L8**: IC_{50} = 3.3 nM; **L9**: IC_{50} = 3.5 nM). Upon 5-Cl substitution of **L7** switched into 5-Br or 5-F substitution, the potency was significantly decreased (**L10**: IC_{50} = 27.5 nM; **L11**: IC_{50} = 7.8 nM). Replacement of 5-Cl of **L8** with 5-F also caused decreased potency (**L12**: IC_{50} = 9.5 nM).

Further SAR exploration based on the terminal benzene ring (A ring) of **L7** and **L8** was conducted, resulting in compounds **L13**–**L23** (Table 2). Introduction of substituents at the terminal benzene ring generally led to decreased activity. For example, introduction of a *para*-methylsulfonyl group resulted in a big loss of activity (**L13**: IC_{50} > 1 μM). Of note, the compounds with meta-substitution (**L15**: IC_{50} = 6.5 nM) were more potent than the compounds with para-substitution (**L14**: IC_{50} = 56.1 nM).

The hydrophilic D-serine tail of **L7** and related compounds served as hydrogen-bond donors and played an important role in binding with PD-L1. To further investigate the variability of this hydrophilic tail, compounds **L24**–**L42** with various hydrogen-bond donors or acceptors replacing the D-serine moiety were synthesized and biologically evaluated (Table 3). Compound **L24**, an ethyl ester of **L7**, showed significantly decreased potency (IC_{50} = 425.9 nM), indicating the critical role of the free acid group in binding with PD-L1. Compound **L25**, a L-serine analogue of **L7**, showed similar potency (IC_{50} = 2.6 nM) to **L7**, suggesting that the chiral configuration of the serine moiety had little effect on the activity. Other compounds (**L33**–**L42**) with different hydrophilic side chains showed variable potency (IC_{50} = 13.3–3592.5 nM) but were much less potent than **L7**.

Docking Study on L7. Molecular docking was used to predict the binding mode of **L7** (Figure 3). In comparison with the binding mode of **L1**, the different substituted halogens (Br on ring B and Cl on ring C) of **L7** strengthened the conserved π–π stacking interactions with $Tyr56_A$ and $Tyr56_B$. The hydrogen-bonding interactions with $Thr20_A$, $Asp122_A$, and $Lys124_A$ were also kept. The π–π stacking interaction and π-cation interaction dominated the protein–ligand interactions between the benzoxadiazole unit and the pocket surrounded by $Tyr123_A$, $Lys124_A$, and $Arg125_A$, which was different from the binding mode of **L1**. The Glide docking score of **L7** (−13.379 kcal/mol) also indicated the more potent binding affinity of **L7** to PD-L1 (Table S1).

Binding Affinity of L7 to hPD-1 and hPD-L1. The kinetic analysis of the interaction of **L7** with hPD-L1 or hPD-1 was performed through a surface plasmon resonance (SPR) method. As shown in Figure 4, the calculated K_D value for **L7** binding to the hPD-L1 extracellular segment was 3.34 nM. Notably, there was no binding for hPD-1 upon treatment with various concentrations of **L7**, indicating that this compound took effects through binding to PD-L1 but not PD-1.

Cytotoxicity Evaluation. To exclude the cytotoxic effects of the test compounds on the subsequent *in vitro* and *in vivo* assays, the cytotoxicity of the compounds (**L7**, **L8**, **L9**, **L11**,

Table 2. PD-1/PD-L1 Blockade Effect of Compounds L5–L23 with Substitutions on A–C Rings[a]

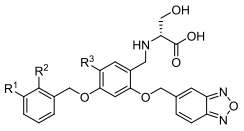

Compound	R^1	R^2	R^3	IC_{50} (nM) HTRF[a]
L5	Ph	CF_3	H	1384.5±167.6
L6	Ph	CH_3	Cl	16.6±1.3
L7	Ph	Br	Cl	1.8±0.4
L8	Ph	Cl	Cl	3.3±1.3
L9	Ph	F	Cl	3.5±0.9
L10	Ph	Br	Br	27.5±1.8
L11	Ph	Br	F	7.8±0.4
L12	Ph	Cl	F	9.5±0.1
L13		Cl	Cl	>1 μM
L14		Cl	Cl	56.1±8
L15		Cl	Cl	6.5±0.9
L16		Cl	Cl	58.7±14.8
L17		Cl	Cl	162.1±5.7
L18	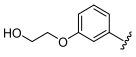	Cl	Cl	101.4±38.8
L19	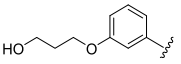	Cl	Cl	60.9±4.2
L20		Br	Cl	8.2±0.4
L21		Br	Cl	7.8±0.4
L22		Br	Cl	24.3±5.5
L23	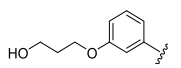	Br	Cl	30.9±7.4

[a]The data were generated from two independent experiments.

https://doi.org/10.1021/acs.jmedchem.1c00392
J. Med. Chem. 2021, 64, 8391–8409

Table 3. PD-1/PD-L1 Blockade Effect of Compounds L24−L42 with Hydrophilic Tail Substitutions[a]

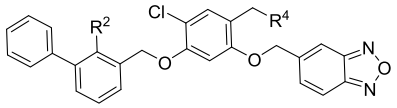

Compound	R^2	R^4	IC_{50} (nM) HTRF[a]
L24	Br	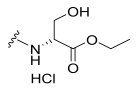	425.9±15.3
L25	Br	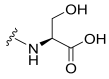	2.6±0.2
L26	Br		13.3±2.1
L27	Br	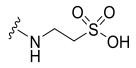	26.9±3.1
L28	Br	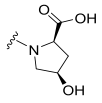	24.3±5.5
L29	Br	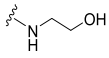	30.8±1.5
L30	Br	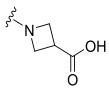	52.3±18.2
L31	Br	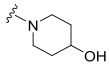	1054.5±299.1
L32	Br		3592.5±1153.3
L33	Br	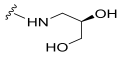	14.6±3.3

Compound	R^2	R^4	IC_{50} (nM) HTRF[a]
L34	Br	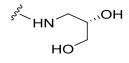	15.9±1.7
L35	Br	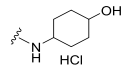	57.2±14.3
L36	Br	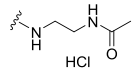	129.8±20.8
L37	Br	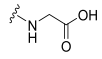	33.7±2.7
L38	Br	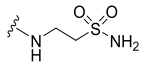	341.7±24.6
L39	Cl	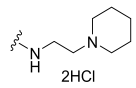	290.9±21.4[b]
L40	Cl	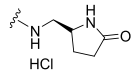	21.6±4.1
L41	Cl	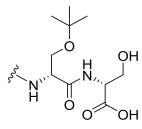	392.9±40.3
L42	Cl	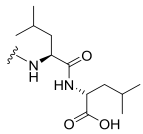	1580.5±133.6

[a]The data were generated from two independent experiments.

L12, **L15**, **L20**, **L21**, **L28**, **BMS-202**, and **BMS-1016**) was evaluated in PD-1$^+$/NFAT-luc/Jurkat cells, PD-L1$^+$/aAPC/CHO-K1 cells, and MC38 cells (Figure S1). In the above cell lines, **L7**, **L9**, **L11**, **L15**, and **L20** did not affect cell viability at various concentrations (0.1−10 μM), while **L8**, **L12**, **L21**, and **L28** only showed slight inhibition of cell viability at 10 μM. Of note, **BMS-202** and **BMS-1016** significantly decreased cell viability at 10 μM. These results indicated that the benzoxadiazole compounds had a lower cytotoxic effect than the BMS compounds, and the influence of cytotoxicity of our compounds on the subsequent cellular assays and *in vivo* antitumor experiments could be excluded.

https://doi.org/10.1021/acs.jmedchem.1c00392
J. Med. Chem. 2021, 64, 8391−8409

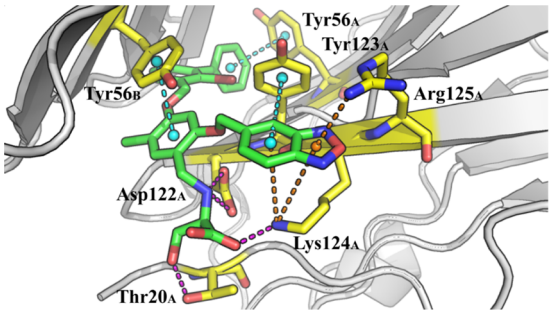

Figure 3. Binding mode of **L7** in the pocket of the PD-L1 dimer predicted by molecular docking (the docking model was based on the dimeric PD-L1 protein taken from PDB ID: 5J89). The $\pi-\pi$ stacking interactions were shown as a cyan dash line, π-cation interactions were shown as an orange dash line, and hydrogen-bonding interactions were shown as a magenta dash line.

Cell-Based PD-1/PD-L1 Signaling Blockade Assay. The cell-based assay was conducted in a coculture system containing PD-1$^+$/NFAT-luc/Jurkat cells and PD-L1$^+$/aAPC/CHO-K1 cells. PD-1$^+$/NFAT-luc/Jurkat cells are T lymphocyte-like cell lines (Jurkat), which are modified by carrying a luciferase reporter gene driven by a T-cell receptor (TCR)-inducible NFAT response element and constitutively express hPD-1. PD-L1$^+$/aAPC/CHO-K1 cells are antigen-presenting surrogate CHO cells, which constitutively express the TCR agonist and hPD-L1. TCR signaling could be transferred from CHO cells to Jurkat cells but repressed by the interaction of PD-1/PD-L1. The compounds that inhibit PD-1/PD-L1 interaction could release the TCR-mediated activation of the Jurkat cells, evidenced by the increased activity of luciferase. The fluorescence intensity is proportional to the inhibition potency. Atezolizumab, a clinically relevant anti-PD-L1 antibody,[22,23] was shown to inhibit the PD-1/PD-L1 interaction with an EC_{50} value of 0.258 nM and a RLU_{max} value of 2.395 (Table 4 and Figure 5A). **L7** exhibited an EC_{50} value of 376 nM and was much potent than **BMS-1016** (EC_{50} = 2075 nM) and **BMS-202** (EC_{50} > 10 000 nM) (Table 4 and Figure 5B). The significant difference in potency of **L7** determined by the HTRF assay (IC_{50} = 1.8 nM) and the cell-based assay (EC_{50} = 376 nM) might be attributed to the differential capability for **L7** to induce PD-L1 dimerization under assay conditions. In the HTRF assay, the PD-L1 protein was dissolved in the buffer, which could be more easily dimerized upon contacting with **L7**, while in the cell coculture assay, the extracellular segment of PD-L1 was fixed on the cell membrane, thus requiring more binding force to induce dimerization.

Table 4. Data of Cell-Based PD-1/PD-L1 Signaling Blockade Assay[a]

compound	EC_{50} (nM)	RLU_{MAX}
atezolizumab	0.258 ± 0.043	2.40 ± 0.261
L7	375 ± 84.3	1.81 ± 0.028
BMS-1016	2075 ± 573	1.83 ± 0.079
BMS-202	>10 000	ND[b]

[a]The data were generated from two independent experiments. [b]ND = not determined.

Pharmacokinetic Studies. Given the fact that **L7** exhibited promising potency at both protein and cellular levels, we examined the *in vivo* pharmacokinetic (PK) properties of **L7** and its ester prodrug **L24**. As shown in Table 5, although the PK parameters of **L7** intravenously administered in male Sprague−Dawley (SD) rats were reasonable, this compound had very poor oral bioavailability (0.35%). This might be due to its low cellular permeability (data not shown). To improve the oral exposure of **L7**, we examined the PK property of **L24**, a potential prodrug of **L7**. As expected, **L24** was readily converted into **L7** *in vivo* (Table 5 and Figure S2). Notably, oral administration of **L24** resulted in a significant increase in bioavailability of **L7** (9.12% in SD rats; 7.70% in C57BL/6 mice). Moreover, oral half-lives of **L24** detected in the form of **L7** were 3.43 h in SD rats and 1.55 h in mice. Together, **L7** could be orally bioavailable through its ester prodrug **L24** and could readily achieve plasma concentrations above the cellular efficacious threshold.

Toxicity Studies. Before moving on to the *in vivo* antitumor experiments, we examined the safety profiles of **L24** and **L7**. Acute and subacute toxicity studies on **L24** were conducted in healthy C57BL/6 mice. In an acute toxicity study, oral administration of **L24** at a single dose of 2000 mg/kg resulted in no mortality and obvious body weight loss during the 30 days observation period (Figure S3). In subacute toxicity study, multidose administration of **L24** for 30 days did not lead to mortality, body weight loss, organ (liver, kidneys, lungs, heart, and brain) weight changes, or macroscopic pathologic findings at any dose levels (50, 100, and 300 mg/kg) (Figure S4). Notably, the spleen weight slightly decreased in the low- and medium-dose groups (data not shown), implying possible immunomodulatory effects of the compound. Serum indicators such as aspartate aminotransferase (AST), alanine aminotransferase (ALT), creatine kinase (CK),

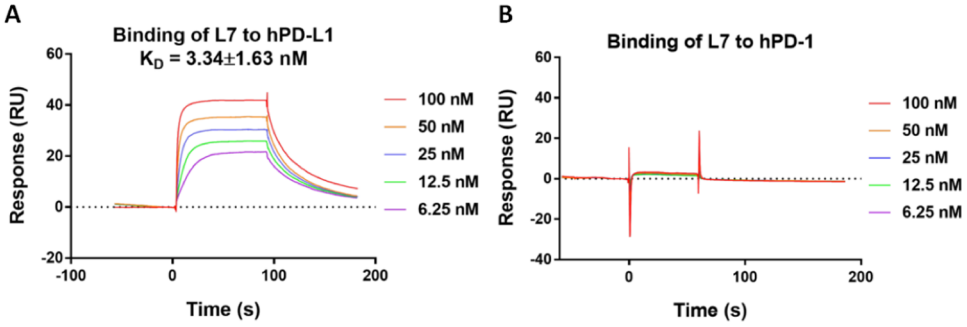

Figure 4. Binding affinity of **L7** to His-hPD-L1 (A) and Fc-hPD-1 (B) was evaluated using the SPR technique. His-hPD-L1 or Fc-hPD-1 was captured on CM5 Chips and various concentrations of **L7** flowed through it. The K_D values were determined by Biacore Evaluation software as mean±SEM from two to three independent experiments.

https://doi.org/10.1021/acs.jmedchem.1c00392
J. Med. Chem. 2021, 64, 8391−8409

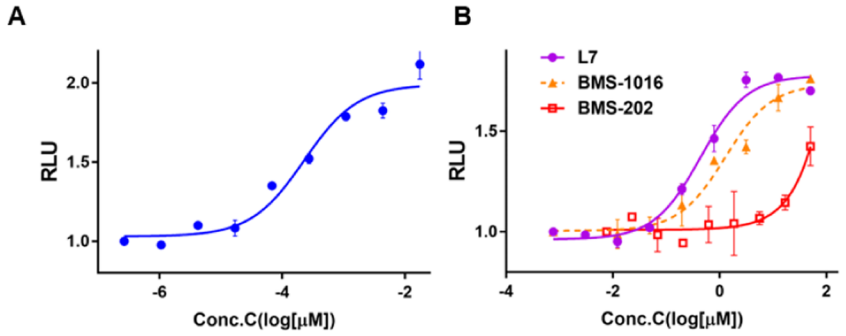

Figure 5. Cell-based PD-1/PD-L1 signaling blockade assay. PD-L1 antibody atezolizumab (A) and small-molecule inhibitors (**L7**, **BMS-1016**, **BMS-202**) (B) were evaluated for their cellular blockade activity on PD-1/PD-L1 interaction in PD-L1$^+$/aAPC/CHO-K1 cells cocultured with PD-1$^+$/NFAT-luc/Jurkat cells for 6 h in the presence of varying concentrations of each inhibitor. The relative potency of the bioactivity assay was expressed as the ratio of EC_{50} determined on the basis of the fitting curve.

Table 5. Pharmacokinetic Parameters of L7 and L24[a]

compound	L7		L24[b]			
species	SD rat		SD rat		C57BL/6 mice	
dosage	2 mg/kg (iv)	10 mg/kg (po)	9 mg/kg (iv)	45 mg/kg (po)	2 mg/kg (iv)	10 mg/kg (po)
$t_{1/2}$ (h)	4.04 ± 0.58	4.17 ± 0.03	5.02 ± 0.36	3.43 ± 0.53	2.05 ± 0.19	1.55 ± 0.26
T_{MAX} (h)	0.08	2.33 ± 3.18	0.08	4	0.08	1
C_{MAX} (ng/mL)	2087 ± 583	4.46 ± 2.06	12971 ± 577	488 ± 79.7	2821 ± 308	150 ± 27
AUC_{0-t} (h·ng/mL)	860 ± 233	15.2 ± 5.50	6280 ± 218	2863 ± 517	1153 ± 100	444 ± 71
CL (mL/h/kg)	2377 ± 534		1426 ± 48.5		1722 ± 144	
F (%)		0.35 ± 0.13		9.12 ± 1.65		7.70 ± 1.24

[a]The data were generated as mean ± SEM (n = 3). [b]The detection form was **L7**. $t_{1/2}$, terminal elimination half-life; T_{MAX}, peak time; C_{MAX}, peak concentration; AUC, area under drug time curve; CL, clearance; F, oral bioavailability.

and blood urea nitrogen (BUN) did not change significantly (Figures S4–S6). H&E staining of major tissues demonstrated no significant toxic effects (data not shown). To further evaluate the potential cardiotoxicity of **L7**, the hERG assay was conducted and showed that **L7** had no inhibitory effect on the hERG potassium channel (IC_{50} > 30 μM). Together, **L24** together with **L7** had very good safety profiles.

Antitumor Efficacy in Tumor Models of Syngeneic Mice. Based on the promising results of the above studies on the selected compounds, we evaluated the *in vivo* antitumor effects of **L24** in B16-F10 melanoma and MC38 colon cancer models of C57BL/6J mice. In the B16-F10 melanoma model, tumor implantation and treatment started on the same day (day 1). **L24** (15 mg/kg, 45 mg/kg) and cyclophosphamide (CTX, 80 mg/kg) were administered via oral gavage once a day for 18 days. As shown in Figure 6, the tumor volume was significantly reduced from day 11. After 18 days of treatment, the average tumor growth inhibition (TGI) rates of the **L24**-treated groups were 45.77% (15 mg/kg group) and 70.70% (45 mg/kg group) (Figure 6A). The average tumor weights of the **L24**-treated groups were 1.27 g (15 mg/kg group) and 0.79 g (45 mg/kg group), compared to 1.76 g of the vehicle control (Figure 6B). The CTX-treated group (positive control) showed much better tumor growth inhibition than the **L24**-treated groups, but CTX caused severe weight loss in mice due to its toxicity (Figure 6C). In contrast, **L24**-treated mice exhibited stable body weights and spleen weights (Figure 6C,D). Together, **L24** exhibited a significant preventive antitumor effect against melanoma tumor growth.

In the MC38 colon cancer model, after the implanted tumor reached 50 mm^3, the treatment started (day 1). As shown in Figure 7, on day 14, **L24** showed a significant antitumor effect at low dosage (50 mg/kg) (TGI = 50.93%) and medium dosage (150 mg/kg) (TGI = 58.17%) but not at high dosage (300 mg/kg) (TGI = 36.47%). On day 18, all three dosages exhibited significant antitumor efficacy, although the high-dosage regimen (TGI = 48.88%) was still less effective than the medium-dosage regimen (TGI = 55.09%). In fact, we have repeated this kind of *in vivo* antitumor experiments many times, and the phenomenon that higher-dosage regimens might not end up with better antitumor efficacy did exist. Notably, the results from phase II clinical trials on PD-L1/VISTA dual inhibitor **CA-170** indicated that a higher incidence of clinical benefits and irAEs was observed at a lower dosage (400 mg) instead of a higher dosage (800 mg) (https://www.curis.com/pipeline/ca-170/). These findings suggested that higher-dosage regimens of small-molecule immunostimulatory agents might not result in more effective antitumor immunity. Further studies on the dose–efficacy relationship and the underlying mechanisms are ongoing in our laboratory.

Antitumor Efficacy in the PD-L1 Humanized Tumor Mouse Model. Our findings demonstrated that **L24** exhibited significant antitumor effects via its active metabolite **L7** in syngeneic mouse tumor models. Although other studies confirmed the antitumor effect of BMS compound analogues in syngeneic mouse models,[16] we thought that such syngeneic models might be insufficient to evaluate the *in vivo* antitumor activity of **L24**, considering that human PD-L1 (hPD-L1) has 77% sequence homology with mouse PD-L1 (mPD-L1).[24] In fact, we found that **L7** had no binding to mPD-L1 in the SPR assay (Figure S7). Therefore, we hoped to evaluate the antitumor activity of **L24** in PD-L1-humanized tumor models to recapitulate human biology.[25] PD-L1-humanized MC38 cells (MC38-hPD-L1) and PD-L1-humanized mice were

https://doi.org/10.1021/acs.jmedchem.1c00392
J. Med. Chem. 2021, 64, 8391–8409

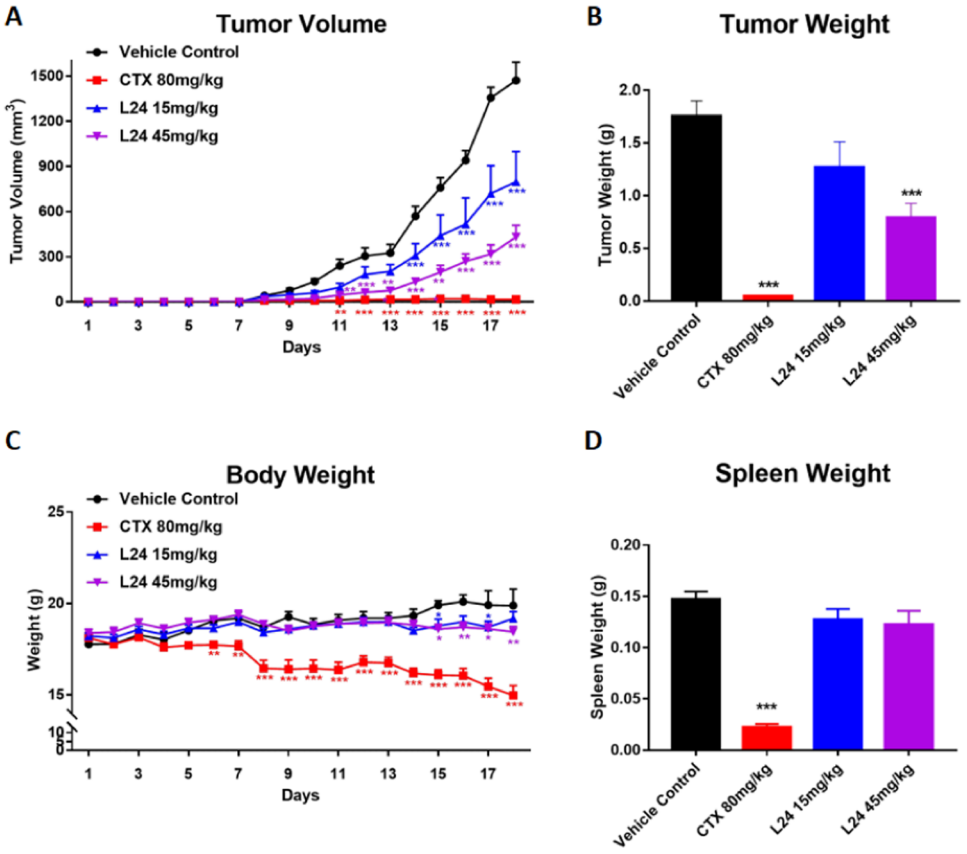

Figure 6. L24 treatment inhibited tumor growth in the B16-F10 melanoma mouse model. B16-F10 melanoma tumors were established by injecting 1×10^6 B16-F10 cells into the dorsal area of mice. Treatment with CMC-Na (vehicle), **L24**, or CTX started on the same day when the tumor cells were injected (day 1). On day 18, the mice were sacrificed and the tumors were isolated. The tumor volume curve (A), tumor weight (B), body weight (C), and spleen weight (D) of the tumor-bearing mice are presented. For tumor volume and body weight, statistical analysis was performed by two-way analysis of variance (ANOVA) multiple comparisons. For tumor weight and spleen weight, statistical analysis was performed by one-way ANOVA multiple comparisons. All quantitative data were represented as means ± SEM (n = 8−10); *p < 0.1, **p < 0.01, and ***p < 0.001 vs vehicle group.

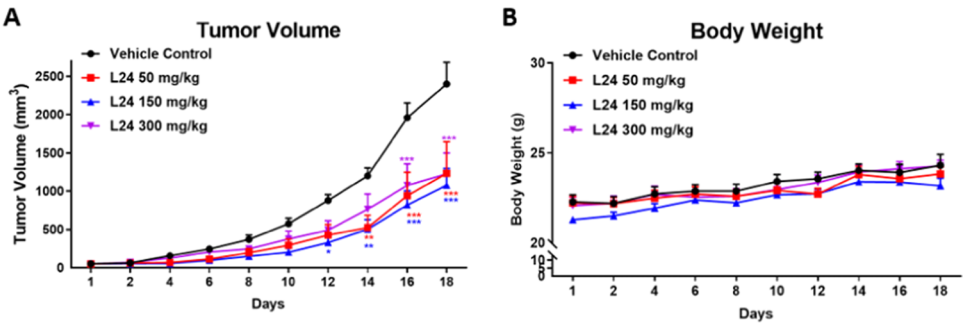

Figure 7. L24 treatment inhibited tumor growth in the MC38 colon cancer mouse model. C57BL/6 mice were injected with 1×10^6 MC38 cells into the dorsal area. When the tumor volume reached 50 mm^3, the mice bearing tumors were randomly divided into four groups and treated with CMC-Na (vehicle), **L24** (50 mg/kg), **L24** (150 mg/kg), and **L24** (300 mg/kg) by oral gavage daily. After 18 days of treatment, the mice were sacrificed and the tumors were isolated. Tumor volume curve (A) and body weight (B) of the tumor-bearing mice are presented. Statistical analysis was performed by two-way ANOVA multiple comparisons. All quantitative data were represented as means ± SEM (n = 8−10); *p < 0.1, **p < 0.01, and ***p < 0.001 vs vehicle group.

constructed by replacing mouse PD-L1 extracellular segment with the same part of human PD-L1. Tumor implantation was carried out by injection of MC38-hPD-L1 cells into PD-L1 humanized C57BL/6 mice. As shown in Figure 8, **L24** exhibited significant antitumor efficacy in this model with TGIs of 44.2% at a dose of 25 mg/kg and 30.8% at a dose of 50 mg/kg. Interestingly, two tumor volume curves crossed during the period of treatment. High dosage (50 mg/kg) showed a stronger antitumor effect in the early stage of administration, while after day 23, low dosage (25 mg/kg) exhibited a better effect. This phenomenon suggests that the dosage of **L24** might be a key factor for its antitumor effect.

To further investigate the optimal dosage, a lower dosage was used in the PD-L1 humanized tumor mouse model. As shown in Figure 9, on the last day of treatment, **L24** exhibited significant antitumor efficacy at a dose of 25 mg/kg (TGI =

https://doi.org/10.1021/acs.jmedchem.1c00392
J. Med. Chem. 2021, 64, 8391−8409

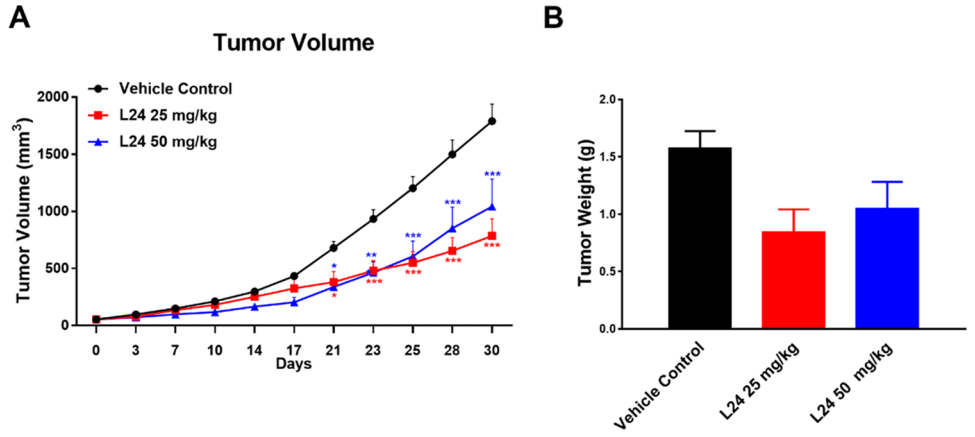

Figure 8. L24 inhibited tumor growth in the PD-L1 humanized tumor mouse model. PD-L1 humanized C57BL/6 mice were injected with 1×10^6 MC38-hPD-L1(Tg)-mPDL1(KO) cells into the right flank area. When the tumor volume reached 50 mm^3, the mice bearing tumors were randomly divided into three groups and treated with CMC-Na (vehicle) and **L24** (25 and 50 mg/kg) by oral gavage daily. After 30 days of treatment, the mice were sacrificed and the tumors were isolated. Tumor volume curve (A) and tumor weight (B) are presented. Statistical analysis was performed by two-way ANOVA multiple comparisons. All quantitative data were represented as means ± SEM ($n = 6$); $^*p < 0.05$ and $^{***}p < 0.001$ vs vehicle control group.

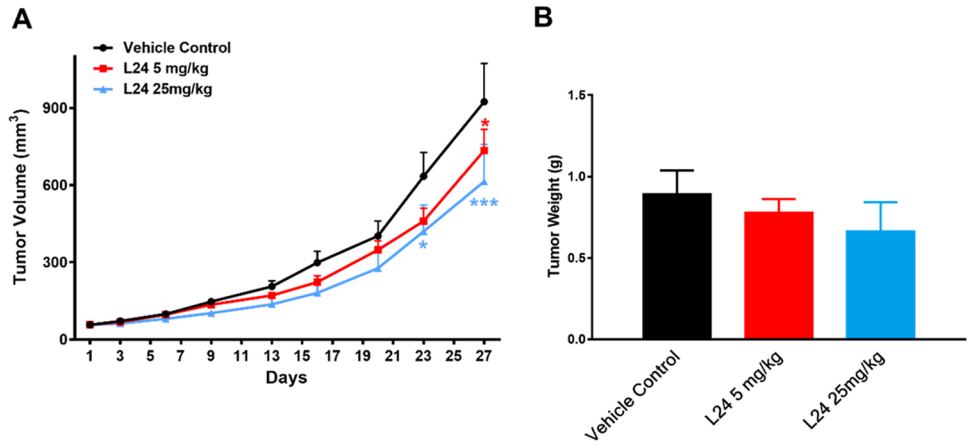

Figure 9. L24 treatment inhibited tumor growth in PD-L1 humanized tumor mouse model. PD-L1 humanized C57BL/6 mice were injected with 1×10^6 MC38-hPD-L1(Tg)-mPDL1(KO) cells into the right flank area. When the tumor volume reached 50 mm^3, the mice bearing tumors were randomly divided into three groups and treated with CMC-Na (vehicle) and **L24** (5 and 25 mg/kg) by oral gavage daily. After 27 days of treatment, the mice were sacrificed and the tumors were isolated. Tumor volume curve (A) and tumor weight (B) are presented. Statistical analysis was performed by two-way ANOVA multiple comparisons. All quantitative data were represented as means ± SEM ($n = 8$); $^*p < 0.05$ and $^{***}p < 0.001$ vs vehicle control group.

32.5%) but not at a dose of 5 mg/kg (TGI = 19.3%). Of note, in the 25 mg/kg dosage group, one mouse exhibited complete tumor regression.

To investigate the mechanism of the antitumor effect of **L24**, cell counts for T-cell subsets, myeloid-derived suppressor cell (MDSC) subsets, macrophages (MΦs), and natural killer (NK) cells in tumor tissues were determined by flow cytometry. As shown in Figure 10, **L24** treatment altered the phenotype of tumor-infiltrating immune cells. The $CD3^+$ T cells were increased in the 25 mg/kg dosage group compared to the vehicle and 5 mg/kg dosage groups. Among $CD3^+$ T cells in the 25 mg/kg dosage group, the ratio of $CD8^+$ T cells to $CD4^+$ T cells increased. (Figure 11). NK cells play an important role in killing tumor cells as a result of the antitumor immune response,[26,27] and it was found that the percentage of NK cells increased in the 25 mg/kg dosage group (Figure 10). On the other hand, immunosuppressive cells, such as MDSC subsets and tumor-associated macrophages (TAMs), are critical players within the immunosuppressive microenvironment.[28,29] We found that **L24** (25 mg/kg) was able to reduce the proportions of mMDSCs (monocytic MDSCs), gMDSCs (granulocytic MDSCs), and macrophages ($CD11b^+F4/80^+$) (Figure 10). However, no significant changes in regulatory T (Treg) cells were observed (Figure 10). Together, **L24** suppressed tumor growth probably through modulating the proportions of tumor-infiltrating lymphocytes (TILs) with upregulated cytotoxic T and NK cells and downregulated immunosuppressive cells.

CONCLUSIONS

In this study, using **BMS-1016** as a lead compound, a series of novel benzoxadiazole derivatives have been designed, synthesized, and biologically evaluated as PD-L1 inhibitors. SAR analysis and docking studies suggested that the benzoxadiazole unit and the serine side chain played key roles in binding with PD-L1. Among the selected compounds, **L7** (HTRF assay: IC_{50} = 1.8 nM; cell coculture assay: EC_{50} = 375 nM) exhibited much more potent PD-1/PD-L1 blockade activity than **BMS-**

https://doi.org/10.1021/acs.jmedchem.1c00392
J. Med. Chem. 2021, 64, 8391−8409

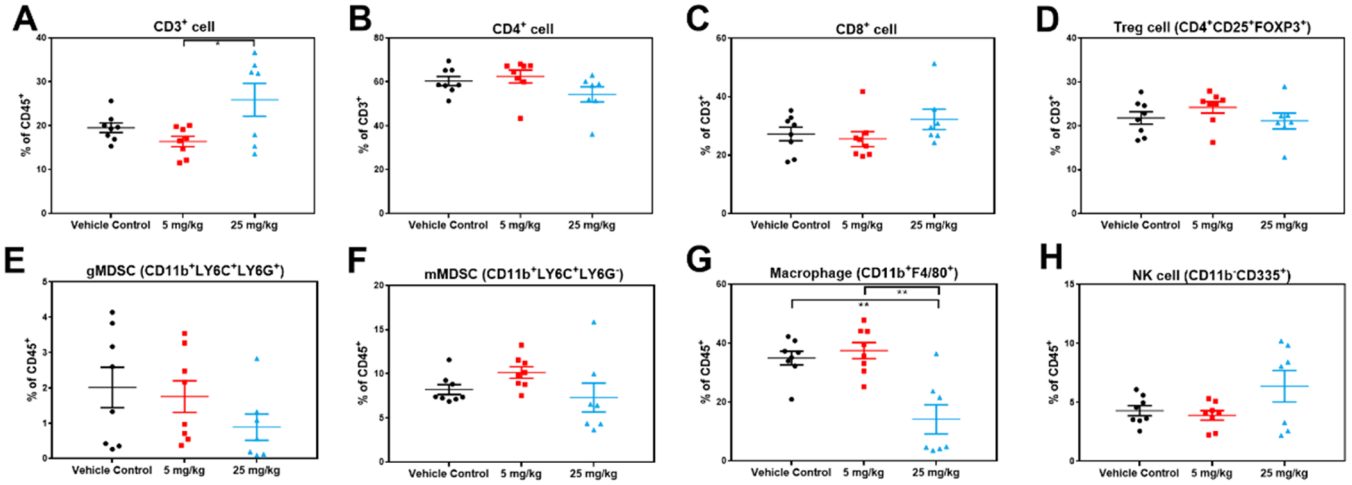

Figure 10. Flow cytometry analysis of the lymphocyte profile within the tumor. Plots showing abundance of $CD3^+$ T cells (A), $CD4^+$ T cells (B), $CD8^+$ T cells (C), Treg cells (D), gMDSCs (E), mMDSCs (F), macrophages (G), and NK cells (h). Statistical analysis was performed by one-way ANOVA multiple comparisons. All quantitative data were represented as means ± SEM (n = 7−8); $^*p < 0.05$ and $^{**}p < 0.01$. mMDSC, monocytic MDSC; gMDSC, granulocytic MDSC.

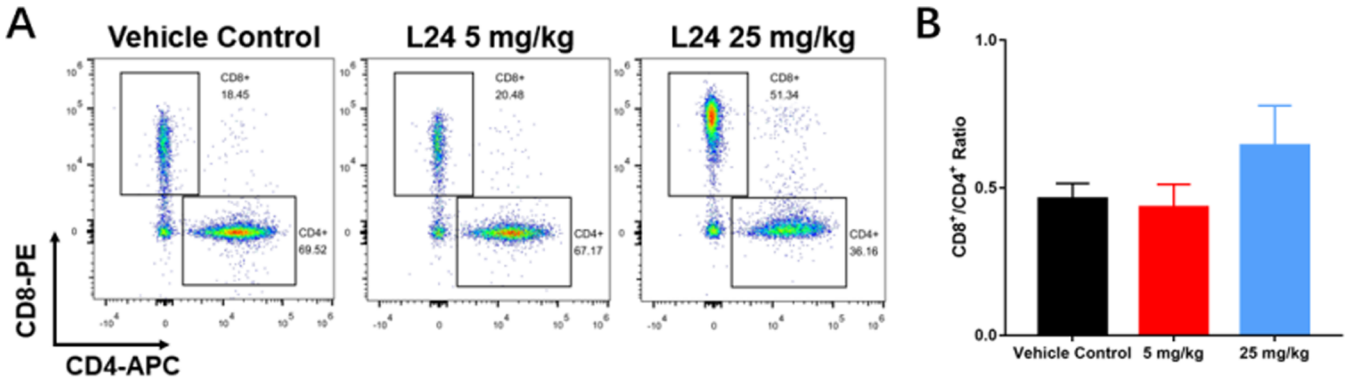

Figure 11. (A) Flow cytometry analysis of $CD4^+$T cells and $CD8^+$ T cells within tumor tissues of representative individuals from three groups (vehicle control, **L24** 5 mg/kg and **L24** 25 mg/kg). (B) Ratio of $CD8^+$ T cells to $CD4^+$ T cells. The data were represented as means ± SEM (n = 7−8).

1016 (HTRF assay: IC_{50} = 35.8 nM; cell coculture assay: EC_{50} = 2075 nM) at protein and cellular levels. Binding affinity assay results showed that **L7** had strong binding to hPD-L1 (SPR assay: K_D = 3.34 nM) without binding to hPD-1. PK studies demonstrated that **L7** was orally bioavailable in the form of its ester prodrug **L24**. Importantly, **L24** exhibited significant antitumor effects in tumor models of syngeneic and PD-L1-humanized mice. Preliminary mechanistic studies indicated that promotion of the antitumor immune response might contribute to the antitumor effects of **L24**. Given the good safety profiles of **L24** and **L7**, this class of benzoxadiazole PD-L1 inhibitors holds promise for small-molecule-based tumor immunotherapy.

EXPERIMENTAL SECTION

General Chemistry. Reagents and solvents were purchased from commercial suppliers and used as received without further purification. All of the reactions were monitored by analytical thin-layer chromatography (TLC) using silica gel 60 F254 plates (Qingdao Ocean Chemical Company, China). Silica gel column chromatography was performed using silica gel (200−300 mesh, Qingdao Ocean Chemical Company, China). ^{1}H NMR spectra were recorded on an ACF* 300Q Bruker spectrometer. ^{1}H NMR chemical shifts are reported in ppm relative to tetramethylsilane (TMS) with the solvent resonance employed as the internal standard ($CDCl_3$ at 7.26 ppm, DMSO-d_6 at 2.50 ppm). Proton coupling patterns were described as follows: singlet (s), doublet (d), doublet of doublets (dd), triplet (t), triplet of doublets (td), quartet (q), multiplet (m), and broad (br). ^{13}C NMR chemical shifts are reported in ppm from tetramethylsilane (TMS) with the solvent resonance as the internal standard ($CDCl_3$ at 77.20 ppm, DMSO-d_6 at 39.51 ppm). The purity of all target compounds was more than 95% as confirmed by a Waters ACQUITY UPLC with a BEH C18 column (2.1 × 50 mm^2, 1.7 μm). The elution condition was a linear gradient from 0 to 100% B over 2 min and then 100% B for 3 min (A = H_2O, B = MeOH with 0.1% AcOH, flow rate 0.3 mL/min).

*(2-(Benzo[c][1,2,5]oxadiazol-5-ylmethoxy)-4-((2-methyl-[1,1′-biphenyl]-3-yl)methoxy)benzyl)-D-serine (**L1**).* Compound **11a** (see the Supporting Information, SI) (292 mg, 0.65 mmol) was added into a solution of D-serine ethyl ester hydrochloride (330 mg, 1.95 mmol), ethyldiisopropylamine (DIPEA, 323 μL, 1.95 mmol), and one drop of glacial acetic acid in anhydrous DCM (4 mL). The solution was stirred at room temperature for 2 h. Sodium triacetoxyborohydride (612 mg, 2.76 mmol) was then added into the reaction mixture and stirred at room temperature for approximately 20 h. The reaction mixture was concentrated under reduced pressure, and saturated $NaHCO_3$ (10 mL) was added, which was then extracted with DCM (3 × 20 mL). The combined organic layer was washed with water (3 × 30 mL) and brine (20 mL), dried over Na_2SO_4, filtered, and concentrated. The resulting residue was purified by flash chromatography (DCM/MeOH = 50:1) to get a yellow solid (150 mg). The

https://doi.org/10.1021/acs.jmedchem.1c00392
J. Med. Chem. 2021, 64, 8391−8409

yellow solid was dissolved in MeOH (5 mL), and lithium hydroxide (22 mg, 0.52 mmol) was added to react at room temperature for 6 h. The mixture was concentrated under reduced pressure, and water (3 mL) was added. The pH value was adjusted to 7 by 1 N HCl. The resulted precipitate was filtered, washed with water, and dried to yield a white solid (132 mg, 13% for two steps) ^{1}H NMR (300 MHz, DMSO-d_6) δ 8.17 (s, 1H), 8.07 (d, J = 9.3 Hz, 1H), 7.73 (dd, J = 9.3, 1.3 Hz, 1H), 7.49−7.41 (m, 3H), 7.40−7.33 (m, 2H), 7.32−7.27 (m, 2H), 7.27−7.14 (m, 2H), 6.87 (d, J = 2.3 Hz, 1H), 6.73 (dd, J = 8.4, 2.3 Hz, 1H), 5.33 (s, 2H), 5.15 (s, 2H), 4.10 (d, J = 5.3 Hz, 2H), 3.75 (dd, J = 11.2, 4.6 Hz, 1H), 3.64 (dd, J = 11.2, 6.6 Hz, 1H), 3.20 (dd, J = 6.6, 4.6 Hz, 1H), 2.17 (s, 3H). ^{13}C NMR (126 MHz, DMSO-d_6) δ 142.65, 142.46, 141.81, 134.34, 133.10, 132.47, 130.10, 129.62, 128.71, 128.41, 127.43, 127.43, 125.95, 116.73, 113.20, 106.76, 101.07, 69.18, 62.73, 61.01, 45.76, 16.30. HRMS (ESI): exact mass calculated for $C_{31}H_{30}N_3O_6$ [M + H]$^+$ 540.21291, found 540.21305. Purity, 96.47%.

*(2-(Benzo[c][1,2,5]oxadiazol-4-ylmethoxy)-4-((2-methyl-[1,1′-biphenyl]-3-yl)methoxy)benzyl)-D-serine (**L2**).* **L2** was prepared starting with compound **11b** (see SI) according to the procedure described for preparation of **L1** to yield a white solid (48 mg, 26% for two steps). ^{1}H NMR (300 MHz, DMSO-d_6) δ 8.01 (d, J = 9.0 Hz, 1H), 7.79 (d, J = 6.5 Hz, 1H), 7.66−7.58 (m, 1H), 7.44 (d, J = 7.2 Hz, 3H), 7.41−7.34 (m, 2H), 7.31 (d, J = 7.8 Hz, 2H), 7.22 (dd, J = 18.0, 7.5 Hz, 2H), 6.96 (s, 1H), 6.73 (d, J = 7.9 Hz, 1H), 5.58 (s, 2H), 5.17 (s, 2H), 4.08 (s, 2H), 3.71 (dd, J = 5.6 Hz, 1H), 3.62 (dd, J = 5.6 Hz, 1H), 3.20 (t, J = 5.5 Hz, 1H), 2.18 (s, 3H). ^{13}C NMR (126 MHz, DMSO-d_6) δ 169.10, 160.78, 157.81, 149.55, 148.09, 142.66, 135.84, 134.38, 133.21, 132.80, 130.36, 130.13, 129.63, 128.71, 128.46, 127.44, 125.98, 115.92, 114.60, 107.09, 100.99, 69.21, 66.35, 63.05, 60.53, 45.55, 16.32. HRMS (ESI): exact mass calculated for $C_{31}H_{30}N_3O_6$ [M + H]$^+$ 540.21291, found 540.21309. Purity, 95.77%.

*(2-(Benzo[c][1,2,5]thiadiazol-5-ylmethoxy)-5-chloro-4-((2-methyl-[1,1′-biphenyl]-3-yl)methoxy)benzyl)-D-serine (**L3**).* **L3** was prepared starting with compound **11c** (see the SI) according to the procedure described for the preparation of **L1** to yield a white solid (126 mg, 23% for two steps). ^{1}H NMR (300 MHz, DMSO-d_6) δ 8.23 (s, 1H), 8.11 (d, J = 9.0 Hz, 1H), 7.86 (dd, J = 9.1, 1.7 Hz, 1H), 7.50−7.36 (m, 5H), 7.34−7.27 (m, 2H), 7.26−7.15 (m, 2H), 6.91 (d, J = 2.3 Hz, 1H), 6.75 (dd, J = 8.4, 2.3 Hz, 1H), 5.42 (s, 2H), 5.17 (s, 2H), 4.24 (s, 2H), 3.90 (dd, J = 12.0, 3.3 Hz, 1H), 3.81 (dd, J = 12.0, 4.3 Hz, 1H), 3.75 (d, J = 3.8 Hz, 1H), 2.17 (s, 3H). ^{13}C NMR (126 MHz, DMSO-d_6) δ 169.06, 161.09, 158.20, 154.79, 142.66, 141.78, 139.51, 135.75, 133.64, 130.34, 130.12, 129.61, 128.71, 128.43, 127.43, 125.94, 121.75, 119.61, 106.85, 100.99, 69.53, 69.20, 60.90, 59.31, 44.22, 16.29. HRMS (ESI): exact mass calculated for $C_{31}H_{30}N_3O_5S$ [M + H]$^+$ 556.19007, found 556.19012. Purity, 98.54%.

*(2-(Benzofuran-6-ylmethoxy)-4-((2-methyl-[1,1′-biphenyl]-3-yl)methoxy)benzyl)-D-serine (**L4**).* **L4** was prepared starting with compound **11d** (see the SI) according to the procedure described for the preparation of **L1** to yield a white solid (20 mg, 23% for two steps). ^{1}H NMR (300 MHz, DMSO-d_6) δ 8.00 (d, J = 2.2 Hz, 1H), 7.83 (d, J = 1.7 Hz, 1H), 7.60 (d, J = 8.5 Hz, 1H), 7.51−7.34 (m, 6H), 7.33−7.28 (m, 2H), 7.27−7.17 (m, 2H), 6.92 (dd, J = 18.5, 2.2 Hz, 2H), 6.71 (dd, J = 8.3, 2.3 Hz, 1H), 5.27 (d, J = 2.6 Hz, 2H), 5.15 (s, 2H), 4.18−4.06 (m, 2H), 3.83 (dd, J = 11.6, 3.8 Hz, 1H), 3.73 (dd, J = 11.7, 5.1 Hz, 1H), 3.51 (d, J = 4.5 Hz, 1H), 2.18 (s, 3H). ^{13}C NMR (126 MHz, DMSO-d_6) δ 169.10, 160.87, 158.30, 154.46, 146.96, 142.66, 141.80, 135.82, 134.36, 132.92, 131.79, 130.13, 129.62, 128.71, 128.46, 127.77, 127.44, 125.98, 124.90, 121.31, 111.69, 107.27, 106.48, 101.08, 70.37, 69.14, 61.73, 59.86, 45.00, 16.30. HRMS (ESI): exact mass calculated for $C_{33}H_{32}NO_6$ [M + H]$^+$ 538.2224, found 538.2225. Purity, 97.21%.

*(2-(Benzo[c][1,2,5]oxadiazol-5-ylmethoxy)-4-((2-(trifluoromethyl)-[1,1′-biphenyl]-3-yl)methoxy)benzyl)-D-serine (**L5**).* **L5** was prepared starting with compound **14a** (see the SI) according to the procedure described for the preparation of **L1** to yield a white solid (12 mg, 20% for two steps). ^{1}H NMR (300 MHz, DMSO-d_6) δ 8.11 (s, 1H), 8.05 (d, J = 9.4 Hz, 1H), 7.74 (t, J = 7.6 Hz, 2H), 7.66 (t, J = 7.7 Hz, 1H), 7.48−7.36 (m, 3H), 7.36−7.20 (m, 4H), 6.77 (d, J = 2.3 Hz, 1H), 6.60 (dd, J = 8.5, 2.1 Hz, 1H), 5.29 (s, 2H), 5.26 (s, 2H), 3.74 (d, J = 3.1 Hz, 2H), 3.48 (dd, J = 13.9, 5.6 Hz, 1H), 3.35 (dd, J = 13.9, 7.1 Hz, 2H), 2.76 (dd, J = 7.8, 5.6 Hz, 1H). ^{13}C NMR (126 MHz, DMSO-d_6) δ 174.83, 174.49, 158.98, 157.23, 149.33, 142.78, 142.45, 136.53, 133.07, 132.71, 132.12, 131.18, 130.30, 128.68, 128.36, 127.95, 125.48 (q, J = 28.5 Hz), 125.05 (d, J = 276.7 Hz), 120.66, 116.73, 113.01, 106.23, 100.99, 69.00, 68.17, 62.80, 46.49, 23.76. HRMS (ESI): exact mass calculated for $C_{31}H_{27}F_3N_3O_6$ [M + H]$^+$ 594.1846, found 594.1842. Purity, 96.18%.

*(2-(Benzo[c][1,2,5]oxadiazol-5-ylmethoxy)-5-chloro-4-((2-methyl-[1,1′-biphenyl]-3-yl)methoxy)benzyl)-D-serine (**L6**).* **L6** was prepared starting with compound **14b** (see the SI) according to the procedure described for the preparation of **L1** to yield a white solid (19 mg, 21% for two steps). ^{1}H NMR (300 MHz, DMSO-d_6) δ 8.15 (s, 1H), 8.08 (d, J = 9.2 Hz, 1H), 7.73 (d, J = 9.4 Hz, 1H), 7.54−7.43 (m, 4H), 7.39 (d, J = 6.9 Hz, 1H), 7.31 (d, J = 7.3 Hz, 2H), 7.25−7.15 (m, 2H), 7.14 (s, 1H), 5.40 (s, 2H), 5.27 (s, 2H), 3.93 (s, 2H), 3.59 (d, J = 5.8 Hz, 2H), 3.06 (s, 1H), 2.22 (s, 3H). ^{13}C NMR (126 MHz, DMSO-d_6) δ 171.98, 156.13, 154.36, 149.35, 142.65, 142.32, 141.73, 135.47, 133.00, 131.47, 130.21, 129.63, 128.72, 128.26, 127.44, 125.94, 119.19, 116.81, 113.51, 113.29, 100.89, 70.12, 69.69, 62.91, 62.00, 45.37, 16.32. HRMS (ESI): exact mass calculated for $C_{31}H_{29}ClN_3O_6$ [M + H]$^+$ 574.17394, found 574.17529. Purity, 98.19%.

*(2-(Benzo[c][1,2,5]oxadiazol-5-ylmethoxy)-4-((2-bromo-[1,1′-biphenyl]-3-yl)methoxy)-5-chlorobenzyl)-D-serine (**L7**).* **L7** was prepared starting with compound **14c** (see the SI) according to the procedure described for the preparation of **L1** to yield a white solid (36 mg, 24% for two steps). ^{1}H NMR (300 MHz, DMSO-d_6) δ 8.15 (s, 1H), 8.07 (d, J = 9.3 Hz, 1H), 7.72 (d, J = 9.3 Hz, 1H), 7.64−7.59 (m, 1H), 7.53 (s, 1H), 7.52−7.42 (m, 4H), 7.41−7.30 (m, 3H), 7.09 (s, 1H), 5.40 (s, 2H), 5.30 (s, 2H), 3.99 (s, 2H), 3.75−3.55 (m, 2H), 3.17 (t, J = 5.5 Hz, 1H). ^{13}C NMR (126 MHz, DMSO-d_6) δ 170.33, 155.80, 154.01, 148.87, 148.59, 143.00, 141.77, 140.74, 136.25, 132.50, 131.45, 131.07, 129.22, 128.81, 128.16, 127.74, 127.70, 122.78, 117.68, 116.36, 113.12, 112.89, 100.38, 71.02, 69.29, 62.67, 60.98, 44.58. HRMS (ESI): exact mass calculated for $C_{30}H_{26}BrClN_3O_6$ [M + H]$^+$ 640.06676, found 640.06584. Purity, 95.71%.

*(2-(Benzo[c][1,2,5]oxadiazol-5-ylmethoxy)-5-chloro-4-((2-chloro-[1,1′-biphenyl]-3-yl)methoxy)benzyl)-D-serine (**L8**).* **L8** was prepared starting with compound **14d** (see the SI) according to the procedure described for the preparation of **L1** to yield a white solid (12 mg, 20% for two steps). ^{1}H NMR (300 MHz, DMSO-d_6) δ 8.15 (s, 1H), 8.07 (d, J = 9.1 Hz, 1H), 7.71 (d, J = 9.5 Hz, 1H), 7.64 (d, J = 6.2 Hz, 1H), 7.54 (s, 1H), 7.51−7.35 (m, 7H), 7.12 (s, 1H), 5.40 (s, 2H), 5.34 (s, 2H), 4.01 (s, 2H), 3.74−3.60 (m, 2H), 3.21 (t, J = 5.4 Hz, 1H). ^{13}C NMR (126 MHz, DMSO-d_6) δ 156.24, 149.35, 142.26, 135.12, 132.99, 131.70, 129.74, 129.21, 128.72, 128.27, 127.66, 118.51, 116.81, 113.33, 100.91, 69.74, 69.07, 62.95, 61.52, 45.04. HRMS (ESI): exact mass calculated for $C_{30}H_{26}Cl_2N_3O_6$ [M + H]$^+$ 594.11932, found 594.11915. Purity, 95.13%.

*(2-(Benzo[c][1,2,5]oxadiazol-5-ylmethoxy)-5-chloro-4-((2-fluoro-[1,1′-biphenyl]-3-yl)methoxy)benzyl)-D-serine (**L9**).* **L9** was prepared starting with compound **14e** (see the SI) according to the procedure described for the preparation of **L1** to yield a white solid (23 mg, 21% for two steps). ^{1}H NMR (300 MHz, DMSO-d_6) δ 8.14 (s, 1H), 8.07 (d, J = 9.3 Hz, 1H), 7.70 (d, J = 9.2 Hz, 1H), 7.59−7.40 (m, 8H), 7.28 (t, J = 7.6 Hz, 1H), 7.15 (s, 1H), 5.40 (s, 2H), 5.36 (s, 2H), 4.02 (s, 2H), 3.72−3.63 (m, 2H), 3.24 (t, 1H). ^{13}C NMR (126 MHz, DMSO-d_6) δ 157.53 (d, J = 248.9 Hz), 156.20, 154.39, 149.34, 142.22, 135.27, 132.93, 131.71, 131.41, 129.92, 129.32, 129.30, 129.12, 128.86 (d, J = 13.2 Hz), 128.45, 125.16, 124.50 (d, J = 15.5 Hz), 116.79, 113.59, 113.18, 100.90, 69.68, 65.54, 63.02, 61.56, 45.07. HRMS (ESI): exact mass calculated for $C_{30}H_{26}ClFN_3O_6$ [M + H]$^+$ 578.14887, found 578.14837. Purity, 99.12%.

*(2-(Benzo[c][1,2,5]oxadiazol-5-ylmethoxy)-5-bromo-4-((2-bromo-[1,1′-biphenyl]-3-yl)methoxy)benzyl)-D-serine (**L10**).* **L10** was prepared starting with compound **14f** (see the SI) according to the procedure described for preparation of **L1** to yield a white solid

https://doi.org/10.1021/acs.jmedchem.1c00392
J. Med. Chem. 2021, 64, 8391−8409

(28 mg, 26% for two steps). 1H NMR (300 MHz, DMSO-d_6) δ 8.16 (s, 1H), 8.07 (d, J = 9.3 Hz, 1H), 7.73 (d, J = 9.5 Hz, 1H), 7.70−7.62 (m, 2H), 7.54−7.41 (m, 4H), 7.41−7.31 (m, 3H), 7.07 (s, 1H), 5.41 (s, 2H), 5.30 (s, 2H), 4.00 (s, 2H), 3.71−3.61 (m, 2H), 3.17 (d, J = 5.5 Hz, 1H). ^{13}C NMR (126 MHz, DMSO-d_6) δ 170.85, 156.93, 155.39, 149.36, 149.08, 143.45, 142.27, 141.22, 136.79, 134.67, 133.01, 131.47, 129.71, 129.14, 128.64, 128.22, 128.16, 123.09, 119.08, 116.85, 113.40, 102.31, 100.80, 71.50, 69.69, 63.04, 61.53, 45.04. HRMS (ESI): exact mass calculated for $C_{30}H_{26}Br_2N_3O_6$ [M + H]$^+$ 684.01624, found 684.01634. Purity, 98.16%.

*(2-(Benzo[c][1,2,5]oxadiazol-5-ylmethoxy)-4-((2-bromo-[1,1′-biphenyl]-3-yl)methoxy)-5-fluorobenzyl)-D-serine (**L11**).* **L11** was prepared starting with compound **14g** (see the SI) according to the procedure described for the preparation of **L1** to yield a white solid (18 mg, 21% for two steps). ^{1}H NMR (300 MHz, DMSO-d_6) δ 8.14 (s, 1H), 8.07 (d, J = 9.3 Hz, 1H), 7.70 (d, J = 9.3 Hz, 1H), 7.59 (d, J = 7.3 Hz, 1H), 7.51−7.40 (m, 4H), 7.41−7.31 (m, 4H), 7.12 (d, J = 7.1 Hz, 1H), 5.35 (s, 2H), 5.29 (s, 2H), 3.98 (s, 2H), 3.69−3.61 (m, 2H), 3.17 (t, 1H). ^{13}C NMR (126 MHz, DMSO-d_6) δ 170.74, 152.94, 149.34, 149.05, 146.57 (d, J = 11.6 Hz), 146.54 (d, J = 237.2 Hz), 143.54, 142.40, 141.24, 136.68, 133.01, 131.69, 129.75, 129.66, 128.61, 128.19, 128.15, 123.64, 118.30 (d, J = 20.2 Hz), 117.13, 116.77, 113.27, 102.15, 71.87, 70.00, 63.03, 61.44, 45.00. HRMS (ESI): exact mass calculated for $C_{30}H_{26}BrFN_3O_6$ [M + H]$^+$ 624.09631, found 624.09704. Purity, 96.70%.

*(2-(Benzo[c][1,2,5]oxadiazol-5-ylmethoxy)-4-((2-chloro-[1,1′-biphenyl]-3-yl)methoxy)-5-fluorobenzyl)-D-serine (**L12**).* **L12** was prepared starting with compound **14h** (see the SI) according to the procedure described for the preparation of **L1** to yield a white solid (55 mg, 26% for two steps). ^{1}H NMR (300 MHz, DMSO-d_6) δ 8.14 (s, 1H), 8.07 (d, J = 9.3 Hz, 1H), 7.70 (d, J = 9.3 Hz, 1H), 7.64−7.58 (m, 1H), 7.52−7.34 (m, 8H), 7.15 (d, J = 7.2 Hz, 1H), 5.35 (s, 2H), 5.33 (s, 2H), 4.01 (s, 2H), 3.73−3.61 (m, 2H), 3.21 (t, J = 5.3 Hz, 1H). ^{13}C NMR (126 MHz, DMSO-d_6) δ 170.43, 153.02, 149.36, 149.06, 147.49, 146.74, 146.64, 145.60, 142.39, δ 140.24 (d, J = 245.8 Hz), 135.05, 133.01, 131.89, 131.45, 129.74, 129.71, 128.72, 128.28, 127.66, 118.47, 118.31, 116.76, 113.26, 102.15, 70.00, 69.45, 63.00, 61.28, 44.91. HRMS (ESI): exact mass calculated for $C_{30}H_{26}ClFN_3O_6$ [M + H]$^+$ 578.14887, found 578.14936. Purity, 98.19%.

*(2-(Benzo[c][1,2,5]oxadiazol-5-ylmethoxy)-5-chloro-4-((2-chloro-4′-(methylsulfonyl)-[1,1′-biphenyl]-3-yl)methoxy)benzyl)-D-serine (**L13**).* **L13** was prepared starting with compound **18a** (see the SI) according to the procedure described for the preparation of **L1** to yield a white solid (30 mg, 20% for two steps). ^{1}H NMR (300 MHz, DMSO-d_6) δ 8.15 (s, 1H), 8.06 (t, J = 8.0 Hz, 3H), 7.72 (d, J = 8.5 Hz, 4H), 7.54 (s, 1H), 7.52−7.39 (m, 2H), 7.12 (s, 1H), 5.41 (s, 2H), 5.36 (s, 2H), 4.01 (s, 2H), 3.67 (m, J = 11.0, 5.3 Hz, 2H), 3.18 (t, J = 5.3 Hz, 1H). ^{13}C NMR (126 MHz, DMSO-d_6) δ 172.96, 156.14, 154.05, 149.41, 149.12, 144.37, 142.42, 141.13, 139.75, 135.71, 132.85, 131.43, 131.15, 130.76, 130.71, 129.94, 127.76, 127.23, 127.18, 116.78, 114.71, 113.43, 102.42, 70.27, 70.21, 69.53, 69.47, 63.25, 62.49, 45.64, 44.18, 44.13. HRMS (ESI): exact mass calculated for $C_{31}H_{28}Cl_2N_3O_8S$ [M + H]$^+$ 672.0969, found 672.0967. Purity, 98.87%.

*(2-(Benzo[c][1,2,5]oxadiazol-5-ylmethoxy)-5-chloro-4-((2-chloro-4′-fluoro-[1,1′-biphenyl]-3-yl)methoxy)benzyl)-D-serine (**L14**).* **L14** was prepared starting with compound **18b** (see the SI) according to the procedure described for the preparation of **L1** to yield a white solid (26 mg, 19% for two steps). ^{1}H NMR (300 MHz, DMSO-d_6) δ 8.14 (s, 1H), 8.07 (d, J = 9.2 Hz, 1H), 7.72 (d, J = 9.3 Hz, 1H), 7.64 (d, J = 6.7 Hz, 1H), 7.53 (s, 1H), 7.51−7.37 (m, 4H), 7.32 (m, J = 8.8 Hz, 2H), 7.11 (s, 1H), 5.40 (s, 2H), 5.33 (s, 2H), 3.98 (s, 2H), 3.73−3.58 (m, 2H), 3.16 (t, 1H). ^{13}C NMR (126 MHz, DMSO-d_6) δ 171.15, 162.25 (d, J = 244.4 Hz), 156.22, 154.34, 149.34, 149.05, 142.28, 140.10, 135.53, 135.20, 132.97, 131.93, 131.79 (d, J = 18.9 Hz), 131.16, 129.33, 127.69, 118.81, 116.81, 115.71, 115.54, 113.58, 113.31, 100.92, 69.73, 69.03, 63.01, 61.66, 45.13. HRMS (ESI): exact mass calculated for $C_{30}H_{25}Cl_2FN_3O_6$ [M + H]$^+$ 612.10990, found 612.10784. Purity, 97.91%.

*(2-(Benzo[c][1,2,5]oxadiazol-5-ylmethoxy)-5-chloro-4-((2-chloro-3′-fluoro-[1,1′-biphenyl]-3-yl)methoxy)benzyl)-D-serine-(**L15**).* **L15** was prepared starting with compound **18c** (see the SI) according to the procedure described for the preparation of **L1** to yield a white solid (33 mg, 24% for two steps). ^{1}H NMR (300 MHz, DMSO-d_6) δ 8.14 (s, 1H), 8.06 (d, J = 9.3 Hz, 1H), 7.70 (d, J = 9.5 Hz, 1H), 7.65 (d, J = 7.0 Hz, 1H), 7.58−7.48 (m, 2H), 7.46−7.37 (m, 2H), 7.31−7.22 (m, 3H), 7.11 (s, 1H), 5.39 (s, 2H), 5.33 (s, 2H), 4.02 (s, 2H), 3.74−3.60 (m, 2H), 3.25 (t, J = 5.3 Hz, 1H). ^{13}C NMR (126 MHz, DMSO-d_6) δ 170.46, 162.26 (d, J = 243.6 Hz), 156.28, 154.47, 149.34, 149.05, 142.23, 141.39 (d, J = 7.6 Hz), 139.81, 135.23, 132.97, 131.89, 131.65, 130.99, 130.75 (d, J = 8.5 Hz), 129.61, 127.75, 126.08, 118.15, 116.80, 116.71 (d, J = 23.4 Hz), 115.19 (d, J = 21.2 Hz), 113.59, 113.33, 100.89, 69.75, 68.98, 63.01, 61.37, 44.95. HRMS (ESI): exact mass calculated for $C_{30}H_{25}Cl_2FN_3O_6$ [M + H]$^+$ 612.10990 or 614.10695, found 614.10838. Purity, 98.97%.

*(2-(Benzo[c][1,2,5]oxadiazol-5-ylmethoxy)-5-chloro-4-((2-chloro-3′-hydroxy-[1,1′-biphenyl]-3-yl)methoxy)benzyl)-D-serine (**L16**).* **L16** was prepared starting with compound **18d** (see the SI) according to the procedure described for the preparation of **L1** to yield a white solid (36 mg, 22% for two steps). ^{1}H NMR (300 MHz, DMSO-d_6) δ 9.60 (s, 1H), 8.16 (s, 1H), 8.07 (d, J = 9.2 Hz, 1H), 7.71 (d, J = 9.3 Hz, 1H), 7.62 (d, J = 7.2 Hz, 1H), 7.54 (s, 1H), 7.45−7.31 (m, 2H), 7.26 (t, J = 7.9 Hz, 1H), 7.12 (s, 1H), 6.87−6.74 (m, 3H), 5.40 (s, 2H), 5.33 (s, 2H), 4.02 (s, 2H), 3.76−3.60 (m, 2H), 3.22 (t, 1H). ^{13}C NMR (126 MHz, DMSO-d_6) δ 170.33, 157.61, 156.34, 154.61, 149.36, 149.07, 142.19, 141.31, 140.48, 135.04, 132.99, 132.00, 131.54, 131.08, 129.75, 129.13, 127.56, 120.35, 117.75, 116.81, 116.68, 115.24, 113.62, 113.36, 100.89, 69.77, 69.11, 63.04, 61.26, 44.91. HRMS (ESI): exact mass calculated for $C_{30}H_{26}Cl_2N_3O_7$ [M + H]$^+$ 610.11423, found 610.11387. Purity, 99.05%.

*(2-(Benzo[c][1,2,5]oxadiazol-5-ylmethoxy)-5-chloro-4-((2-chloro-2′,3′-difluoro-[1,1′-biphenyl]-3-yl)methoxy)benzyl)-D-serine (**L17**).* **L17** was prepared starting with compound **18e** (see the SI) according to the procedure described for the preparation of **L1** to yield a white solid (8 mg, 19% for two steps). ^{1}H NMR (300 MHz, DMSO-d_6) δ 8.21 (s, 1H), 8.11 (d, J = 9.0 Hz, 1H), 7.91−7.82 (m, 1H), 7.77−7.68 (m, 1H), 7.61−7.49 (m, 2H), 7.49−7.41 (m, 2H), 7.40−7.30 (m, 1H), 7.22 (t, J = 6.8 Hz, 1H), 7.15 (s, 1H), 5.46 (s, 2H), 5.35 (s, 2H), 3.99 (s, 2H), 3.72−3.61 (m, 2H), 3.19 (t, 1H). ^{13}C NMR (126 MHz, DMSO-d_6) δ 172.94, 156.32, 154.94, 154.61, 153.99, 150.49 (dd, J = 246.3, 13.0 Hz), 147.60 (dd, J = 246.7, 12.3 Hz), 139.66, 135.52, 134.42, 132.16, 131.75, 131.02, 130.30, 130.11, 129.24 (d, J = 12.8 Hz), 127.64, 127.13, 125.24, 122.63, 121.78, 119.53, 117.81 (d, J = 17.1 Hz), 114.57, 102.52, 70.55, 69.44, 63.26, 62.48, 45.63. HRMS (ESI): exact mass calculated for $C_{30}H_{24}O_6N_3Cl_2F_2$ [M + H]$^+$ 630.10047, found 630.09869. Purity, 95.70%.

*(2-(Benzo[c][1,2,5]oxadiazol-5-ylmethoxy)-5-chloro-4-((2-chloro-3′-(2-hydroxyethoxy)-[1,1′-biphenyl]-3-yl)methoxy)benzyl)-D-serine (**L18**).* **L18** was prepared starting with compound **18f** (see the SI) according to the procedure described for the preparation of **L1** to yield a white solid (29 mg, 33% for two steps). ^{1}H NMR (300 MHz, DMSO-d_6) δ 8.16 (s, 1H), 8.08 (d, J = 9.3 Hz, 1H), 7.72 (d, J = 9.4 Hz, 1H), 7.68−7.60 (m, 2H), 7.48−7.32 (m, 3H), 7.14 (s, 1H), 7.04−6.84 (m, 3H), 5.41 (s, 2H), 5.36 (s, 2H), 4.16 (s, 2H), 4.04 (t, J = 4.9 Hz, 2H), 3.89−3.76 (m, 2H), 3.73 (t, J = 4.8 Hz, 2H), 3.60 (t, 1H). ^{13}C NMR (126 MHz, DMSO-d_6) δ 169.63, 158.87, 156.65, 155.09, 149.34, 149.06, 142.08, 141.03, 140.50, 135.00, 132.99, 132.84, 131.66, 131.13, 129.82, 129.26, 127.60, 121.99, 116.76, 115.94, 115.50, 114.36, 113.57, 113.40, 100.71, 70.05, 69.83, 69.10, 62.15, 60.18, 60.01, 44.15. HRMS (ESI): exact mass calculated for $C_{32}H_{30}Cl_2N_3O_8$ [M + H]$^+$ 654.1404, found 654.1402. Purity, 96.47%.

*(2-(Benzo[c][1,2,5]oxadiazol-5-ylmethoxy)-5-chloro-4-((2-chloro-3′-(3-hydroxypropoxy)-[1,1′-biphenyl]-3-yl)methoxy)-benzyl)-D-serine (**L19**).* **L19** was prepared starting with compound **18g** (see the SI) according to the procedure described for the preparation of **L1** to yield a white solid (47 mg, 26% for two steps). ^{1}H NMR (300 MHz, DMSO-d_6) δ 8.16 (s, 1H), 8.08 (d, J = 9.3 Hz, 1H), 7.72 (dd, J = 9.3 Hz, 1H), 7.64 (dd, 1H), 7.55 (s, 1H), 7.48−

https://doi.org/10.1021/acs.jmedchem.1c00392
J. Med. Chem. 2021, 64, 8391−8409

7.31 (m, 3H), 7.12 (s, 1H), 7.05−6.89 (m, 3H), 5.41 (s, 2H), 5.35 (s, 2H), 4.09 (t, J = 6.4 Hz, 2H), 4.03 (s, 2H), 3.80−3.61 (m, 2H), 3.57 (t, J = 6.2 Hz, 2H), 3.21 (t, 1H), 1.96−1.73 (m, 2H). ^{13}C NMR (126 MHz, DMSO-d_6) δ 170.19, 158.88, 156.39, 154.71, 149.34, 149.05, 142.18, 141.04, 140.54, 135.07, 132.99, 132.19, 131.62, 131.08, 129.81, 129.20, 127.60, 121.93, 117.19, 116.79, 115.86, 114.36, 113.60, 113.38, 100.84, 69.80, 69.07, 65.16, 63.22, 61.10, 57.79, 44.88, 32.60. HRMS (ESI): exact mass calculated for $C_{33}H_{32}Cl_2N_3O_8$ [M + H]$^+$ 668.1561, found 668.1559. Purity, 98.90%.

*(2-(Benzo[c][1,2,5]oxadiazol-5-ylmethoxy)-4-((2-bromo-3′-fluoro-[1,1′-biphenyl]-3-yl)methoxy)-5-chlorobenzyl)-D-serine (**L20**).* **L20** was prepared starting with compound **18h** (see the SI) according to the procedure described for the preparation of **L1** to yield a white solid (17 mg, 21% for two steps). ^{1}H NMR (300 MHz, DMSO-d_6) δ 8.16 (s, 1H), 8.08 (d, J = 9.4 Hz, 1H), 7.72 (dd, J = 9.3 Hz, 1H), 7.64 (dd, J = 7.3 Hz, 1H), 7.56−7.45 (m, 3H), 7.37 (d, J = 7.6 Hz, 1H), 7.30−7.19 (m, 3H), 7.10 (s, 1H), 5.40 (s, 2H), 5.31 (s, 2H), 4.02 (s, 2H), 3.76−3.66 (m, 2H), 3.24 (t, 1H). ^{13}C NMR (126 MHz, DMSO-d_6) δ 170.81, 162.18 (d, J = 243.8 Hz), 156.24, 154.39, 149.35, 149.06, 143.40, 142.26, 142.15, 136.85, 132.99, 131.82, 131.47, 130.71, 129.68, 128.25, 126.06, 123.04, 118.51, 116.83, 116.68 (d, J = 22.4 Hz), 115.12 (d, J = 20.4 Hz), 113.58, 113.37, 100.89, 71.40, 69.74, 63.01, 61.50, 45.06. HRMS (ESI): exact mass calculated for $C_{30}H_{25}BrClFN_3O_6$ [M + H]$^+$ 656.0594, found 656.0595. Purity, 96.43%.

*(2-(Benzo[c][1,2,5]oxadiazol-5-ylmethoxy)-4-((2-bromo-3′-methoxy-[1,1′-biphenyl]-3-yl)methoxy)-5-chlorobenzyl)-D-serine (**L21**).* **L21** was prepared starting with compound **18i** (see the SI) according to the procedure described for the preparation of **L1** to yield a white solid (17 mg, 27% for two steps). ^{1}H NMR (300 MHz, DMSO-d_6) δ 8.16 (s, 1H), 8.07 (d, J = 9.3 Hz, 1H), 7.72 (d, J = 9.2 Hz, 1H), 7.61 (d, J = 7.4 Hz, 1H), 7.55 (s, 1H), 7.45 (t, J = 7.6 Hz, 1H), 7.42−7.32 (m, 2H), 7.09 (s, 1H), 6.99 (d, J = 8.4 Hz, 1H), 6.96−6.89 (m, 2H), 5.40 (s, 2H), 5.30 (s, 2H), 4.03 (s, 2H), 3.80 (s, 3H), 3.77−3.62 (m, 2H), 3.25 (t, 1H). ^{13}C NMR (126 MHz, DMSO-d_6) δ 170.54, 159.35, 156.24, 154.44, 149.36, 149.07, 143.33, 142.51, 142.25, 136.71, 133.00, 131.83, 131.47, 129.74, 129.31, 128.11, 123.20, 122.01, 118.36, 116.83, 115.42, 113.69, 113.57, 113.39, 100.88, 71.47, 69.74, 62.98, 61.45, 55.61, 44.98. HRMS (ESI): exact mass calculated for $C_{31}H_{28}BrClN_3O_7$ [M + H]$^+$ 668.0794, found 668.0799. Purity, 97.96%.

*(2-(Benzo[c][1,2,5]oxadiazol-5-ylmethoxy)-4-((2-bromo-3′-chloro-[1,1′-biphenyl]-3-yl)methoxy)-5-chlorobenzyl)-D-serine (**L22**).* **L22** was prepared starting with compound **18j** (see the SI) according to the procedure described for the preparation of **L1** to yield a white solid (12 mg, 20% for two steps). ^{1}H NMR (300 MHz, DMSO-d_6) δ 8.13 (s, 1H), 8.05 (d, J = 9.4 Hz, 1H), 7.72 (d, J = 9.3 Hz, 1H), 7.63 (d, J = 7.7 Hz, 1H), 7.53−7.46 (m, 4H), 7.44 (d, J = 3.0 Hz, 1H), 7.39−7.32 (m, 2H), 7.06 (s, 1H), 5.38 (s, 2H), 5.28 (s, 2H), 3.91 (s, 2H), 3.58 (d, J = 5.9 Hz, 2H), 3.04 (t, J = 5.9 Hz, 1H). ^{13}C NMR (126 MHz, DMSO-d_6) δ 172.86, 156.16, 154.07, 149.42, 149.15, 143.34, 142.42, 142.17, 137.24, 133.37, 132.87, 131.29, 131.21, 130.42, 129.60, 129.47, 128.47, 128.19, 122.88, 122.51, 116.81, 114.73, 113.49, 102.42, 72.01, 70.30, 63.28, 62.46, 45.64. HRMS (ESI): exact mass calculated for $C_{30}H_{24}BrCl_2N_3NaO_6$ [M + Na]$^+$ 694.01177 or 696.00973, found 696.00934. Purity, 97.99%.

*(2-(Benzo[c][1,2,5]oxadiazol-5-ylmethoxy)-4-((2-bromo-3′-(3-hydroxypropoxy)-[1,1′-biphenyl]-3-yl)methoxy)-5-chlorobenzyl)-D-serine (**L23**).* **L23** was prepared starting with compound **18k** (see the SI) according to the procedure described for the preparation of **L1** to yield a white solid (26 mg, 17% for two steps). ^{1}H NMR (300 MHz, DMSO-d_6) δ 8.15 (s, 1H), 8.07 (d, 1H), 7.72 (d, 1H), 7.65−7.51 (m, 2H), 7.50−7.28 (m, 3H), 7.09 (s, 1H), 7.05−6.82 (m, 3H), 5.39 (s, 2H), 5.30 (s, 2H), 4.07 (t, 2H), 4.01 (s, 2H), 3.78−3.66 (m, 2H), 3.64−3.52 (m, 2H), 3.22 (t, 1H), 1.97−1.78 (m, 2H). ^{13}C NMR (75 MHz, DMSO-d_6) δ 171.38, 158.84, 156.17, 154.28, 149.35, 149.07, 143.39, 142.54, 142.28, 136.77, 132.95, 131.39, 129.68, 129.19, 128.07, 123.09, 121.89, 119.57, 116.81, 115.91, 114.36, 113.83, 113.40, 101.21, 71.60, 69.83, 65.27, 63.06, 61.78, 57.84, 45.19, 32.64. HRMS (ESI): exact mass calculated for $C_{33}H_{32}BrClN_3O_8$ [M + H]$^+$ 712.10558 or 714.10354, found 714.10327. Purity, 98.22%.

*Ethyl(2-(benzo[c][1,2,5]oxadiazol-5-ylmethoxy)-4-((2-bromo-[1,1′-biphenyl]-3-yl)methoxy)-5-chlorobenzyl)-D-serinate hydrochloride (**L24**).* A solution of **14c** (120 mg, 0.22 mmol), D-serine ethyl ester hydrochloride (150 mg, 0.88 mmol), and one drop of glacial acetic acid in anhydrous DCM (4 mL) was stirred in an ice bath for 2 h. Sodium triacetoxyborohydride (140 mg, 0.66 mmol) was then added into the reaction mixture and stirred at room temperature for approximately 20 h. The reaction mixture was concentrated under reduced pressure, and the residue was taken up in saturated $NaHCO_3$ (10 mL), which was extracted with DCM (3 × 20 mL). The combined organic layer was washed with water (3 × 30 mL) and brine (20 mL), dried over Na_2SO_4, filtered, and concentrated. The resulting residue was purified by flash chromatography (solvent A, DCM; solvent B, MeOH; 0−40% B) to give a colorless oil. The oil product was added into a hydrochloric acid ethanol solution and precipitated as a white solid. The precipitate was filtered, washed with CH_3OH (1.5 mL), and dried to yield a white solid (32 mg, 21%). ^{1}H NMR (300 MHz, DMSO-d_6) δ 9.45 (d, 2H), 8.19 (s, 1H), 8.11 (d, J = 8.9 Hz, 1H), 7.78−7.67 (m, 2H), 7.63 (dd, J = 7.6, 1.8 Hz, 1H), 7.54−7.42 (m, 4H), 7.42−7.32 (m, 3H), 7.14 (s, 1H), 5.65 (s, 1H), 5.43 (s, 2H), 5.35 (s, 2H), 4.28 (s, 2H), 4.12 (m, J = 10.7, 7.1, 3.8 Hz, 3H), 4.01−3.84 (m, 2H), 1.17 (t, J = 7.1 Hz, 3H). ^{13}C NMR (75 MHz, DMSO-d_6) δ 169.34, 158.72, 157.31, 143.82, 138.41, 135.40, 134.83, 133.26, 131.37, 131.06, 130.30, 129.89, 129.84, 118.45, 115.88, 115.73, 115.36, 102.83, 73.48, 71.88, 64.02, 63.13, 61.18, 45.44, 16.02. HRMS (ESI): exact mass calculated for $C_{32}H_{30}BrClN_3O_6$ [M + H]$^+$ 668.09806, found 668.09807. Purity, 98.29%. Enatiomeric excess (ee), 99.64%, chiral high-performance liquid chromatography (HPLC) analysis: CHIRALCEL ODH0CE-SD069 column, 35 °C, (*n*-hexane/isopropanol/diethylamine = 60:40:0.1), 0.8 mL/min.

*(2-(Benzo[c][1,2,5]oxadiazol-5-ylmethoxy)-4-((2-bromo-[1,1′-biphenyl]-3-yl)methoxy)-5-chlorobenzyl)-L-serine (**L25**).* **L25** was prepared starting with compound **14c** and L-serine ethyl ester hydrochloride according to the procedure described for preparation of **L1** to yield a white solid (19 mg, 23% for two steps). ^{1}H NMR (300 MHz, DMSO-d_6) δ 8.15 (s, 1H), 8.05 (d, J = 9.0 Hz, 1H), 7.71 (d, J = 9.2 Hz, 1H), 7.60 (d, J = 5.2 Hz, 2H), 7.52−7.39 (m, 4H), 7.39−7.28 (m, 3H), 7.10 (s, 1H), 5.40 (s, 2H), 5.29 (s, 2H), 4.11 (s, 2H), 3.83−3.68 (m, 2H), 3.38 (s, 1H). ^{13}C NMR (126 MHz, DMSO-d_6) δ 172.93, 156.18, 154.13, 149.45, 149.17, 143.73, 142.44, 141.47, 137.11, 132.88, 131.37, 131.23, 129.65, 129.10, 128.52, 128.12, 128.05, 123.10, 122.50, 116.82, 114.76, 113.50, 102.43, 72.13, 70.33, 63.32, 62.50, 45.67. HRMS (ESI): exact mass calculated for $C_{30}H_{26}BrClN_3O_6$ [M + H]$^+$ 638.06880 or 640.06676, found 640.06711. Purity, 95.53%.

*(S)-1-(2-(benzo[c][1,2,5]oxadiazol-5-ylmethoxy)-4-((2-bromo-[1,1′-biphenyl]-3-yl)methoxy)-5-chlorobenzyl)piperidine-2-carboxylic acid (**L26**).* **L26** was prepared starting with compound **14c** and L-pipecolate methyl ester according to the procedure described for preparation of **L1** to yield a white solid (12 mg, 30% for two steps). ^{1}H NMR (300 MHz, DMSO-d_6) δ 8.13 (s, 1H), 8.09 (d, J = 9.4 Hz, 1H), 7.64 (td, J = 8.3, 7.5, 1.5 Hz, 2H), 7.53−7.30 (m, 8H), 7.07 (s, 1H), 5.38 (s, 2H), 5.29 (s, 2H), 3.87−3.65 (m, 2H), 3.22 (dd, J = 7.5, 4.3 Hz, 1H), 2.94 (m, J = 11.8 Hz, 1H), 2.41−2.28 (m, 1H), 1.79 (m, 2H), 1.50 (m, 3H), 0.85 (m, J = 6.8 Hz, 1H). ^{13}C NMR (126 MHz, DMSO-d_6) δ 173.81, 156.18, 153.87, 149.33, 143.45, 142.54, 141.22, 136.81, 132.89, 131.71, 131.50, 129.68, 129.27, 128.62, 128.19, 128.16, 119.81, 116.84, 113.73, 113.20, 101.03, 71.48, 69.57, 64.19, 52.82, 49.61, 28.91, 24.74, 22.11. HRMS (ESI): exact mass calculated for $C_{33}H_{30}BrClN_3O_5$ [M + H]$^+$ 662.10519 or 664.10314, found 664.10296. Purity, 99.18%.

*2-((2-(Benzo[c][1,2,5]oxadiazol-5-ylmethoxy)-4-((2-bromo-[1,1′-biphenyl]-3-yl)methoxy)-5-chlorobenzyl)amino)ethane-1-sulfonic acid (**L27**).* **L27** was prepared starting with compound **14c** and 2-aminoethane-1-sulfonic acid according to the Borch reductive amination procedure described for the preparation of **L1** to yield a white solid (28 mg, 21%). ^{1}H NMR (300 MHz, DMSO-d_6) δ 8.62 (s,

https://doi.org/10.1021/acs.jmedchem.1c00392
J. Med. Chem. 2021, 64, 8391−8409

1H), 8.16 (s, 1H), 8.08 (d, J = 9.3 Hz, 1H), 7.74 (d, J = 9.4 Hz, 1H), 7.66−7.55 (m, 2H), 7.52−7.28 (m, 7H), 7.13 (s, 1H), 5.44 (s, 2H), 5.32 (s, 2H), 4.23 (s, 2H), 3.21 (t, J = 6.5 Hz, 2H), 2.82 (t, J = 6.4 Hz, 2H). ^{13}C NMR (126 MHz, DMSO-d_6) δ 156.62, 149.36, 149.07, 142.04, 141.17, 136.51, 133.01, 132.95, 131.62, 129.67, 129.37, 128.63, 128.22, 128.16, 123.36, 116.91, 114.17, 113.57, 113.51, 100.74, 71.54, 69.79, 46.98, 45.00, 44.09. HRMS (ESI): exact mass calculated for $C_{29}H_{26}BrClN_3O_6S$ $[M + H]^+$ 658.04087 or 660.03883, found 660.03822. Purity, 96.13%.

*(2R,4R)-1-(2-(benzo[c][1,2,5]oxadiazol-5-ylmethoxy)-4-((2-bromo-[1,1′-biphenyl]-3-yl)methoxy)-5-chlorobenzyl)-4-hydroxypyrrolidine-2-carboxylic acid (**L28**).* **L28** was prepared starting with compound **14c** and (2*R*,4*R*)-methyl 4-hydroxypyrrolidine-2-carboxylate hydrochloride according to the procedure described for the preparation of **L1** to yield a white solid (20 mg, 30% for two steps). ^{1}H NMR (300 MHz, DMSO-d_6) δ 8.17 (s, 1H), 8.09 (d, J = 9.3 Hz, 1H), 7.72 (d, J = 9.3 Hz, 1H), 7.67−7.61 (m, 2H), 7.53−7.42 (m, 4H), 7.41−7.32 (m, 3H), 7.15 (s, 1H), 5.44 (s, 2H), 5.33 (s, 2H), 4.30 (d, J = 6.7 Hz, 2H), 4.14 (d, J = 13.2 Hz, 1H), 3.93 (s, 1H), 3.25 (d, J = 10.7 Hz, 1H), 3.10−3.02 (m, 1H), 1.99−1.89 (m, 1H), 0.88−0.81 (m, 1H). ^{13}C NMR (126 MHz, DMSO-d_6) δ 171.78, 156.73, 155.21, 149.38, 149.09, 143.51, 142.06, 141.21, 136.62, 133.34, 133.07, 131.63, 129.69, 129.47, 128.64, 128.21, 123.39, 116.92, 113.73, 113.61, 100.84, 71.60, 69.93, 68.46, 65.22, 61.74, 51.93, 38.26. HRMS (ESI): exact mass calculated for $C_{32}H_{28}BrClN_3O_6$ $[M + H]^+$ 664.08445 or 666.08241, found 666.08260. Purity, 96.12%.

*2-((2-(Benzo[c][1,2,5]oxadiazol-5-ylmethoxy)-4-((2-bromo-[1,1′-biphenyl]-3-yl)methoxy)-5-chlorobenzyl)amino)ethan-1-ol (**L29**).* **L29** was prepared starting with compound **14c** and ethanolamine according to the Borch reductive amination procedure described for the preparation of **L1** to yield a white solid (51 mg, 25%). ^{1}H NMR (300 MHz, DMSO-d_6) δ 8.27−7.95 (m, 2H), 7.65 (d, J = 9.7 Hz, 1H), 7.61 (d, J = 7.2 Hz, 1H), 7.53−7.25 (m, 8H), 7.04 (s, 1H), 5.35 (s, 2H), 5.27 (s, 2H), 3.72 (s, 2H), 3.46 (t, J = 5.7 Hz, 2H), 2.57 (t, J = 5.7 Hz, 2H). ^{13}C NMR (126 MHz, DMSO-d_6) δ 173.58, 155.67, 153.30, 149.32, 149.06, 143.44, 142.63, 141.23, 136.93, 132.86, 131.44, 130.44, 129.69, 129.15, 128.62, 128.19, 128.14, 123.37, 123.14, 116.90, 113.61, 113.09, 101.06, 71.46, 69.49, 60.75, 51.45, 47.01. HRMS (ESI): exact mass calculated for $C_{29}H_{26}BrClN_3O_4$ $[M + H]^+$ 594.0790, found 594.0790. Purity, 97.95%.

*1-(2-(Benzo[c][1,2,5]oxadiazol-5-ylmethoxy)-4-((2-bromo-[1,1′-biphenyl]-3-yl)methoxy)-5-chlorobenzyl)azetidine-3-carboxylic acid (**L30**).* **L30** was prepared starting with compound **14c** and 3-azetidinecarboxylic acid according to the Borch reductive amination procedure described for the preparation of **L1** to yield a white solid (8 mg, 19%). ^{1}H NMR (300 MHz, DMSO-d_6) δ 8.13 (s, 1H), 8.10 (d, J = 9.3 Hz, 1H), 7.71 (d, J = 9.3 Hz, 1H), 7.62 (d, J = 7.7 Hz, 1H), 7.52−7.41 (m, 4H), 7.41−7.31 (m, 4H), 7.09 (s, 1H), 5.40 (s, 2H), 5.30 (s, 2H), 3.79 (s, 2H), 3.63 (m, 2H), 3.49 (m, 2H), 3.34−3.27 (m, 1H). HRMS (ESI): exact mass calculated for $C_{31}H_{26}BrClN_3O_5$ $[M + H]^+$ 634.07389 or 636.07184, found 636.07083. Purity, 99.00%.

*1-(2-(Benzo[c][1,2,5]oxadiazol-5-ylmethoxy)-4-((2-bromo-[1,1′-biphenyl]-3-yl)methoxy)-5-chlorobenzyl)piperidin-4-ol (**L31**).* **L31** was prepared starting with compound **14c** and 4-hydroxypiperidine according to the Borch reductive amination procedure described for the preparation of **L1** to yield a white solid (9 mg, 20%). ^{1}H NMR (300 MHz, DMSO-d_6) δ 8.13 (s, 1H), 8.09 (d, J = 9.3 Hz, 1H), 7.70−7.61 (m, 2H), 7.52−7.43 (m, 4H), 7.42−7.32 (m, 4H), 7.09 (s, 1H), 5.39 (s, 2H), 5.30 (s, 2H), 4.59 (s, 1H), 3.62−3.49 (m, 3H), 2.76 (t, 2H), 2.18 (t, 1H), 2.00 (t, J = 7.6 Hz, 1H), 1.79−1.70 (m, 2H), 1.51−1.44 (m, 2H). HRMS (ESI): exact mass calculated for $C_{32}H_{30}BrClN_3O_4$ $[M + H]^+$ 634.1103, found 634.1104. Purity, 96.84%.

*5-((5-((2-Bromo-[1,1′-biphenyl]-3-yl)methoxy)-4-chloro-2-((4-methylpiperazin-1-yl)methyl)phenoxy)methyl)benzo[c][1,2,5]-oxadiazole (**L32**).* **L32** was prepared starting with compound **14c** and 1-methylpiperazine according to the Borch reductive amination procedure described for the preparation of **L1** to yield a white solid (14 mg, 21%). ^{1}H NMR (300 MHz, DMSO-d_6) δ 8.14 (s, 1H), 8.10 (d, J = 9.1 Hz, 1H), 7.69−7.61 (m, 2H), 7.52−7.41 (m, 4H), 7.40−7.31 (m, 4H), 7.09 (s, 1H), 5.39 (s, 2H), 5.29 (s, 2H), 3.51 (s, 2H), 2.29 (s, 3H). HRMS (ESI): exact mass calculated for $C_{32}H_{31}BrClN_4O_3$ $[M + H]^+$ 633.1263, found 633.1263. Purity, 97.26%.

*(R)-3-((2-(benzo[c][1,2,5]oxadiazol-5-ylmethoxy)-4-((2-bromo-[1,1′-biphenyl]-3-yl)methoxy)-5-chlorobenzyl)amino)propane-1,2-diol (**L33**).* **L33** was prepared starting with compound **14c** and (*R*)-3-amino-1,2-propanediol according to the Borch reductive amination procedure described for the preparation of **L1** to yield a white solid (22 mg, 29%). ^{1}H NMR (300 MHz, DMSO-d_6) δ 8.15−8.04 (m, 2H), 7.72−7.59 (m, 2H), 7.52−7.42 (m, 5H), 7.41−7.31 (m, 3H), 7.07 (s, 1H), 5.39 (s, 2H), 5.30 (s, 2H), 4.66 (s, 2H), 3.80 (s, 3H), 3.59 (s, 2H), 2.68 (dd, J = 8.0 Hz, 1H), 2.53 (dd, 1H). HRMS (ESI): exact mass calculated for $C_{30}H_{28}BrClN_3O_5$ $[M + H]^+$ 624.0895, found 624.0884. Purity, 96.27%.

*(S)-3-((2-(benzo[c][1,2,5]oxadiazol-5-ylmethoxy)-4-((2-bromo-[1,1′-biphenyl]-3-yl)methoxy)-5-chlorobenzyl)amino)propane-1,2-diol (**L34**).* **L34** was prepared starting with compound **14c** and (S)-3-amino-1,2-propanediol according to the Borch reductive amination procedure described for the preparation of **L1** to yield a white solid (11 mg, 27%). ^{1}H NMR (300 MHz, DMSO-d_6) δ 8.09 (m, J = 8.9 Hz, 2H), 7.68 (d, J = 9.5 Hz, 1H), 7.63 (d, J = 7.6 Hz, 1H), 7.44 (d, J = 13.5 Hz, 5H), 7.41−7.29 (m, 3H), 7.08 (s, 1H), 5.39 (s, 2H), 5.30 (s, 2H), 3.84 (s, 2H), 3.62 (m, 3H), 2.72 (dd, J = 11.7 Hz, 1H), 2.54 (dd, 1H). ^{13}C NMR (126 MHz, DMSO-d_6) δ 156.78, 155.36, 149.35, 149.07, 143.51, 142.15, 141.21, 136.60, 133.17, 131.59, 129.66, 129.43, 128.61, 128.19, 128.16, 123.38, 116.84, 114.20, 113.65, 113.57, 100.78, 71.59, 69.89, 67.63, 63.89, 50.27, 44.65. HRMS (ESI): exact mass calculated for $C_{30}H_{28}BrClN_3O_5$ $[M + H]^+$ 624.0895, found 624.0902. Purity, 95.76%.

*4-((2-(Benzo[c][1,2,5]oxadiazol-5-ylmethoxy)-4-((2-bromo-[1,1′-biphenyl]-3-yl)methoxy)-5-chlorobenzyl)amino)cyclohexan-1-ol hydrochloride (**L35**).* **L35** was prepared starting with compound **14c** and 4-aminocyclohexanol according to the Borch reductive amination procedure described for the preparation of **L1** to give a colorless oil. The oil product was added to a hydrochloric acid ethanol solution and precipitated as a white solid. The precipitate was filtered, washed with CH_3OH (1.5 mL), and dried to yield a white solid (29 mg, 30%). ^{1}H NMR (300 MHz, DMSO-d_6) δ 8.86 (s, 2H), 8.19 (s, 1H), 8.13 (d, J = 9.3 Hz, 1H), 7.76 (d, J = 9.1 Hz, 1H), 7.69−7.60 (m, 2H), 7.47 (dt, J = 10.9, 7.0 Hz, 4H), 7.41−7.31 (m, 3H), 7.16 (s, 1H), 5.41 (s, 2H), 5.36 (s, 2H), 4.13 (s, 2H), 3.49−3.43 (m, 1H), 3.03−2.89 (m, 1H), 2.05 (d, J = 11.4 Hz, 2H), 1.78 (d, J = 10.0 Hz, 2H), 1.38 (dd, J = 23.2, 9.7 Hz, 2H), 1.19−1.02 (m, 2H). ^{13}C NMR (126 MHz, DMSO-d_6) δ 156.77, 155.41, 149.33, 149.07, 143.55, 142.04, 141.19, 136.60, 133.34, 133.19, 131.61, 129.66, 129.38, 128.62, 128.21, 128.18, 123.37, 116.79, 114.62, 113.94, 113.49, 100.65, 71.58, 69.94, 68.02, 56.15, 42.01, 33.37, 27.06. HRMS (ESI): exact mass calculated for $C_{33}H_{32}BrClN_3O_4$ $[M + H]^+$ 648.1259, found 648.1261. Purity, 97.78%.

*N-(2-((2-(benzo[c][1,2,5]oxadiazol-5-ylmethoxy)-4-((2-bromo-[1,1′-biphenyl]-3-yl)methoxy)-5-chlorobenzyl)amino)ethyl)-acetamide hydrochloride (**L36**).* **L36** was prepared starting with compound **14c** and *N*-(2-aminoethyl)acetamide according to the Borch reductive amination procedure described for the preparation of **L1** to give a colorless oil. The oil product was added to a hydrochloric acid ethanol solution and precipitated as a white solid. The precipitate was filtered, washed with CH_3OH (1.5 mL), and dried to yield a white solid (26 mg, 28%). ^{1}H NMR (300 MHz, DMSO-d_6) δ 9.00 (s, 2H), 8.18 (s, 2H), 8.11 (d, J = 9.4 Hz, 1H), 7.74 (d, J = 9.4 Hz, 1H), 7.67 (s, 1H), 7.62 (d, J = 7.5 Hz, 1H), 7.52−7.41 (m, 4H), 7.40−7.31 (m, 3H), 7.15 (s, 1H), 5.45 (s, 2H), 5.34 (s, 2H), 4.20 (s, 2H), 3.38−3.33 (m, 2H), 3.07−2.94 (m, 2H), 1.81 (s, 3H). ^{13}C NMR (126 MHz, DMSO-d_6) δ 170.56, 156.64, 155.40, 149.37, 149.09, 143.53, 142.17, 141.20, 136.57, 133.10, 133.02, 131.64, 129.69, 129.43, 128.65, 128.23, 128.19, 123.41, 116.88, 114.20, 113.57, 100.74, 71.57, 69.85, 46.75, 44.33, 35.63, 23.04. HRMS (ESI): exact mass calculated for $C_{31}H_{29}BrClN_4O_4$ $[M + H]^+$ 635.1055, found 635.1062. Purity, 98.09%.

*(2-(Benzo[c][1,2,5]oxadiazol-5-ylmethoxy)-4-((2-bromo-[1,1′-biphenyl]-3-yl)methoxy)-5-chlorobenzyl)glycine (**L37**).* **L37** was prepared starting with compound **14c** and glycine methyl ester according

https://doi.org/10.1021/acs.jmedchem.1c00392
J. Med. Chem. 2021, 64, 8391−8409

to the procedure described for the preparation of **L1** to yield a white solid (16 mg, 24% for two steps). ^{1}H NMR (300 MHz, DMSO-d_6) δ 8.16 (s, 1H), 8.09 (d, J = 9.6 Hz, 1H), 7.71 (d, J = 9.6 Hz, 1H), 7.62 (d, J = 7.1 Hz, 1H), 7.53 (s, 1H), 7.46 (dd, J = 12.1, 6.2 Hz, 4H), 7.41−7.31 (m, 3H), 7.10 (s, 1H), 5.40 (s, 2H), 5.31 (s, 2H), 3.99 (s, 2H), 3.15 (s, 2H). ^{13}C NMR (126 MHz, DMSO-d_6) δ 170.66, 156.41, 154.63, 149.42, 149.14, 143.72, 142.32, 141.42, 136.98, 132.85, 131.79, 131.40, 129.61, 129.13, 128.52, 123.13, 119.90, 116.82, 114.71, 113.51, 102.23, 72.10, 70.31, 49.51, 46.07. HRMS (ESI): exact mass calculated for $C_{29}H_{24}BrClN_3O_5$ [M + H]$^+$ 608.0582, found 608.0589. Purity, 97.98%.

*2-((2-(Benzo[c][1,2,5]oxadiazol-5-ylmethoxy)-4-((2-bromo-[1,1′-biphenyl]-3-yl)methoxy)-5-chlorobenzyl)amino)ethane-1-sulfonamide (**L38**).* **L38** was prepared starting with compound **14c** and 2-aminoethanesulfonamide according to the Borch reductive amination procedure described for the preparation of **L1** to yield a white solid (28 mg, 24%). ^{1}H NMR (300 MHz, DMSO-d_6) δ 8.14−8.05 (m, 2H), 7.67 (d, J = 9.5 Hz, 1H), 7.62 (d, J = 6.2 Hz, 1H), 7.53−7.30 (m, 8H), 7.06 (s, 1H), 6.80 (s, 2H), 5.38 (s, 2H), 5.28 (s, 2H), 3.73 (s, 2H), 3.16 (t, J = 7.0 Hz, 2H), 2.92 (t, J = 7.1 Hz, 2H). ^{13}C NMR (126 MHz, DMSO) δ 155.68, 153.35, 149.34, 149.09, 143.47, 142.65, 141.26, 136.94, 132.91, 131.45, 130.33, 129.69, 129.16, 128.62, 128.20, 128.15, 123.41, 123.14, 116.93, 113.70, 113.21, 101.24, 71.52, 69.57, 55.00, 46.71, 43.87. HRMS (ESI): exact mass calculated for $C_{29}H_{27}BrClN_4O_5S$ [M + H]$^+$ 657.0569, found 657.0571. Purity, 97.31%.

*N-(2-(Benzo[c][1,2,5]oxadiazol-5-ylmethoxy)-5-chloro-4-((2-chloro-[1,1′-biphenyl]-3-yl)methoxy)benzyl)-2-(piperidin-1-yl)-ethan-1-amine dihydrochloride (**L39**).* **L39** was prepared starting with compound **14d** and 2-piperidin-1-ylethanamine according to the Borch reductive amination procedure described for the preparation of **L1** to yield a colorless oil. The oil product was added to a hydrochloric acid ethanol solution (4 mL) and precipitated as a white solid. The precipitate was filtered, washed with CH_3OH (1.5 mL), and dried to yield a white solid (17 mg, 26%). ^{1}H NMR (300 MHz, DMSO-d_6) δ 10.69 (s, 1H), 9.58 (s, 2H), 8.22 (s, 1H), 8.11 (d, J = 9.3 Hz, 1H), 7.78 (d, J = 9.3 Hz, 1H), 7.73 (s, 1H), 7.64 (dd, J = 7.3, 1.9 Hz, 1H), 7.54−7.46 (m, 3H), 7.45−7.34 (m, 4H), 7.18 (s, 1H), 5.48 (s, 2H), 5.38 (s, 2H), 4.25 (s, 2H), 3.54−3.42 (m, 6H), 2.91 (t, 2H), 1.87−1.73 (m, 4H), 1.71−1.64 (m, 1H), 1.50−1.33 (m, 1H). ^{13}C NMR (126 MHz, DMSO-d_6) δ 156.55, 155.44, 149.37, 149.07, 142.22, 141.16, 139.20, 134.95, 133.19, 132.85, 131.78, 129.73, 129.32, 128.72, 128.28, 127.66, 116.80, 113.99, 113.54, 100.77, 69.84, 69.16, 53.06, 52.48, 44.57, 41.45, 22.77, 21.57. HRMS (ESI): exact mass calculated for $C_{34}H_{35}Cl_2N_4O_3$ [M + H]$^+$ 617.2081, found 617.2080. Purity, 95.57%.

*(S)-5-(((2-(Benzo[c][1,2,5]oxadiazol-5-ylmethoxy)-5-chloro-4-((2-chloro-[1,1′-biphenyl]-3-yl)methoxy)benzyl)amino)methyl)-pyrrolidin-2-one hydrochloride (**L40**).* **L40** was prepared starting with compound **14d** and (5*S*)-5-(aminomethyl)pyrrolidin-2-one according to the Borch reductive amination procedure described for the preparation of **L1** to yield a colorless oil. The oil product was added to a hydrochloric acid ethanol solution (2 mL) and precipitated as a white solid. The precipitate was filtered, washed with CH_3OH (1.5 mL), and dried to yield a white solid (10 mg, 19%). ^{1}H NMR (300 MHz, DMSO-d_6) δ 9.14 (s, 2H), 8.18 (s, 1H), 8.11 (d, J = 9.3 Hz, 1H), 7.77 (s, 2H), 7.72 (d, J = 9.3 Hz, 1H), 7.64 (dd, 1H), 7.44 (m, J = 16.5, 7.5, 4.3 Hz, 7H), 7.18 (s, 1H), 5.45 (s, 2H), 5.39 (s, 2H), 4.21 (s, 2H), 4.01−3.77 (m, 1H), 3.16−2.90 (m, 2H), 2.25−2.05 (m, 3H), 1.83−1.65 (m, 1H). ^{13}C NMR (126 MHz, DMSO-d_6) δ 176.78, 156.68, 155.42, 149.34, 149.07, 142.11, 141.17, 139.20, 134.97, 133.15, 133.07, 131.77, 131.21, 129.73, 129.29, 128.72, 128.28, 127.67, 116.85, 114.05, 113.64, 113.55, 100.69, 69.87, 69.15, 52.37, 50.52, 44.78, 29.70, 24.94. HRMS (ESI): exact mass calculated for $C_{32}H_{29}Cl_2N_4O_4$ [M + H]$^+$ 603.15604, found 603.15564. Purity, 98.12%.

*N-(2-(benzo[c][1,2,5]oxadiazol-5-ylmethoxy)-5-chloro-4-((2-chloro-[1,1′-biphenyl]-3-yl)methoxy)benzyl)-O-(tert-butyl)-D-seryl-D-serine (**L41**).* **L41** was prepared starting with compound **14d** and ethyl *O*-(*tert*-butyl)-D-seryl-D-serinate according to the Borch reductive amination procedure described for the preparation of **L1** to yield a white solid (28 mg, 21%). ^{1}H NMR (300 MHz, DMSO-d_6) δ 8.18−7.97 (m, 3H), 7.77−7.59 (m, 2H), 7.55−7.29 (m, 8H), 7.09 (s, 1H), 5.38 (s, 2H), 5.33 (s, 2H), 4.21 (t, 1H), 3.79 (s, 2H), 3.73 (m, 1H), 3.54 (m, J = 10.4, 4.1 Hz, 1H), 3.44 (dd, J = 3.9 Hz, 1H), 3.38−3.25 (m, 3H), 3.16 (m, 1H), 1.04 (d, J = 2.8 Hz, 9H). ^{13}C NMR (126 MHz, DMSO-d_6) δ 172.56, 171.66, 155.91, 153.54, 149.31, 149.05, 142.56, 141.11, 139.26, 135.30, 132.83, 131.61, 131.01, 130.86, 129.75, 129.08, 128.72, 128.26, 127.64, 122.81, 116.93, 113.65, 113.06, 101.10, 73.21, 69.49, 69.04, 62.98, 62.51, 62.14, 54.51, 45.92, 27.58. HRMS (ESI): exact mass calculated for $C_{37}H_{39}Cl_2N_4O_8$ [M + H]$^+$ 737.2139, found 737.2141. Purity, 95.96%.

*(2-(Benzo[c][1,2,5]oxadiazol-5-ylmethoxy)-5-chloro-4-((2-chloro-[1,1′-biphenyl]-3-yl)methoxy)benzyl)-L-leucyl-D-leucine (**L42**).* **L42** was prepared starting with compound **14d** and ethyl L-leucyl-D-leucinate according to the Borch reductive amination procedure described for the preparation of **L1** to yield a white solid (29 mg, 25%). ^{1}H NMR (300 MHz, DMSO-d_6) δ 8.06 (t, 3H), 7.72−7.59 (m, 2H), 7.54−7.30 (m, 8H), 7.06 (s, 1H), 5.35 (s, 2H), 5.32 (s, 2H), 4.34−4.20 (m, 1H), 3.65 (dd, J = 33.8, 13.9 Hz, 2H), 3.10−3.01 (m, 1H), 1.77−1.63 (m, 1H), 1.62−1.52 (m, 1H), 1.50 (dd, J = 6.6 Hz, 2H), 1.32 (dd, J = 8.2 Hz, 2H), 0.90−0.67 (m, 12H). ^{13}C NMR (126 MHz, DMSO-d_6) δ 174.95, 174.72, 155.68, 153.35, 149.34, 149.07, 142.62, 141.12, 139.27, 135.34, 132.90, 131.60, 131.02, 130.36, 129.75, 129.06, 128.72, 128.27, 127.63, 123.32, 116.84, 113.66, 113.05, 101.00, 69.49, 69.04, 60.38, 50.51, 45.45, 43.18, 24.87, 24.70, 23.49, 23.34, 22.56, 21.67. HRMS (ESI): exact mass calculated for $C_{39}H_{43}Cl_2N_4O_6$ [M + H]$^+$ 733.2554, found 733.2549. Purity, 96.08%.

*N-(2-(((2-methoxy-6-((2-methyl-[1,1′-biphenyl]-3-yl)methoxy)-pyridin-3-yl)methyl)amino)ethyl)acetamide (**BMS-202**).* **BMS-202** was synthesized according to the procedures described in BMS patents.[18] ^{1}H NMR (300 MHz, DMSO-d_6) δ 7.81 (s, 1H), 7.63 (d, J = 7.9 Hz, 1H), 7.52−7.40 (m, 3H), 7.39 (d, J = 6.9 Hz, 1H), 7.31 (dd, J = 8.2, 1.6 Hz, 2H), 7.25 (d, J = 7.5 Hz, 1H), 7.23−7.13 (m, 1H), 6.43 (d, J = 7.8 Hz, 1H), 5.40 (s, 2H), 3.89 (s, 2H), 3.59 (s, 2H), 3.12 (q, J = 6.2 Hz, 2H), 2.58−2.50 (m, 2H), 2.21 (s, 3H), 1.78 (s, 3H). ^{13}C NMR (126 MHz, DMSO-d_6) δ 169.68, 161.17, 141.88, 141.67, 136.44, 134.25, 129.94, 129.61, 128.68, 128.63, 127.39, 125.91, 113.68, 101.21, 66.61, 53.64, 48.42, 46.40, 38.91, 23.09, 16.37. HRMS (ESI): exact mass calculated for $C_{25}H_{30}N_3O_3$ [M + H]$^+$ 420.2242, found 420.2288. Purity, 99.17%.

*(2-((3-Cyanobenzyl)oxy)-4-((2-methyl-[1,1′-biphenyl]-3-yl)-methoxy)benzyl)-D-serine (**BMS-1016**).* **BMS-1016** was synthesized according to the procedures described in BMS patents.[19] ^{1}H NMR (300 MHz, DMSO-d_6) δ 8.02 (s, 1H), 7.91 (d, J = 7.9 Hz, 1H), 7.81 (d, J = 7.6 Hz, 1H), 7.61 (t, J = 7.8 Hz, 1H), 7.53−7.10 (m, 9H), 6.83 (d, J = 2.2 Hz, 1H), 6.72 (d, J = 8.4 Hz, 1H), 5.25 (s, 2H), 5.15 (s, 2H), 4.16−3.97 (m, 2H), 3.82−3.54 (m, 4H), 3.17 (t, J = 5.7 Hz, 1H), 2.18 (s, 3H). ^{13}C NMR (75 MHz, DMSO-d_6) δ 168.78, 159.99, 157.23, 142.15, 141.31, 138.46, 135.34, 133.82, 132.37, 131.86, 131.63, 130.93, 129.66, 129.58, 129.09, 128.18, 127.91, 126.90, 125.45, 118.63, 115.02, 111.45, 106.13, 100.58, 68.65, 68.50, 62.16, 60.42, 45.24, 15.77. HRMS (ESI): exact mass calculated for $C_{32}H_{31}N_2O_5$ [M + H]$^+$ 523.2188, found 523.2234. Purity, 99.40%.

Docking Method. Molecular docking was completed with Glide 5.5 implemented in Schrödinger2009.[30] The crystal structure (PDB ID: 5J89) of PD-L1 in complex with **BMS-202** was obtained from the Protein Data Bank (http://www.rcsb.org/). The crystal structure was prepared with the Protein Preparation Wizard workflow. All of the water molecules were removed. The grid file for molecular docking was generated based on the binding site, which was defined by a box centered on the centroid of the crystal ligand and in similar size to it. Compounds were prepared with LigPrep and docked using the Glide extra-precision (XP) mode. Default settings were used for all of the other parameters.

PD-1/PD-L1 Homogeneous Time-Resolved Fluorescence (HTRF) Binding Assay. The blockade activity of compounds against PD-1/PD-L1 interaction was determined by the PD-1/PD-L1 binding assay kit (cisbio, 64ICP01PEG). Briefly, the test compound was diluted to a series of appropriate concentrations (0.1 nM to 10 μM)

https://doi.org/10.1021/acs.jmedchem.1c00392
J. Med. Chem. 2021, 64, 8391−8409

by diluent buffer and applied to the 384-well plate in triplicate (2 μL volume). Then, 4 μL of Tag1-PD-L1 protein and 4 μL of Tag2-PD-1 protein were added and incubated for 15 min at room temperature. Then, 10 μL of premixed anti-Tag1-Eu^{3+} and anti-Tag2-XL665 was added and the plate was sealed with 2 h incubation at room temperature. At last, the signals were read on an EnVision multilabel plate reader (PerkinElmer, Waltham, MA) with excitation at 337 nm and emission at 665 and 610 nm. HTRF signals were calculated as a ratio as follows: (signal of 665 nm)/(signal of 615 nm) × 10 000. The inhibition rates and the half-maximal inhibitory concentrations (IC_{50}) were calculated using GraphPad Prism 7.0 version.

Cell Viability Assay. The toxicity of the compounds was tested in PD-$L1^+$/aAPC/CHO-K1 cells and MC38 cells by the methyl thiazolyl tetrazolium (MTT) assay and in PD-1^+/NFAT-luc/Jurkat cells by the CCK8 assay. Test compounds were dissolved in dimethyl sulfoxide (DMSO) and subsequently diluted in a culture medium with a 1% final DMSO concentration. Briefly, PD-$L1^+$/aAPC/CHO-K1 cells or MC38 cells were seeded in 96-well microplates at an appropriate density (PD-$L1^+$/aAPC/CHO-K1, 2000 cells/well; MC38, 5000 cells/well) in 100 μL of medium and allowed to adhere for 12 h. The cells were treated with test compounds and incubated for 24 h. For the PD-1^+/NFAT-luc/Jurkat cell assay, the cells were seeded in 96-well microplates at a density of 20 000 cells per well in 100 μL of medium, treated with the test compounds, and incubated for 24 h. After incubation, CCK8 and MTT were added into the well according to the manufacturer's protocol and incubated for 4 h. The absorbance of the CCK8 assay was read on an automated microplate spectrophotometer (EnSpire, PerkinElmer). In the MTT assay, the culture medium should be replaced with DMSO to test the absorbance. Statistical analysis was carried out using GraphPad Prism 7.0 version.

Cell-Based PD-1/PD-L1 Signaling Blockade Assay. The PD-1^+/NFAT-luc/Jurkat cells and PD-$L1^+$/aAPC/CHO-K1 cells were purchased from Genomeditech (Shanghai, China). Anti-PD-L1 mAb (Atezolizumab) was purchased from Selleckchem (Shanghai, China). The PD-$L1^+$/aAPC/CHO-K1 cells were seeded at a cell density of 25 000 cells/well into 96-well plates 12 h prior to the assay. Compounds were dissolved in diluted culture medium with 1% final DMSO concentration. The culture medium in the wells was removed, and 50 μL of compound dilutions was added. The PD-1^+/NFAT-luc/Jurkat cells were then seeded at 100 000 cells/well in 50 μL of culture medium and incubated at 37 °C and in 5% CO_2 for 6 h. After incubation, Bio-Glo reagent was added to each well, and luminescence was quantified using an automated microplate spectrophotometer (EnSpire, PerkinElmer). EC_{50} values and maximal luminescence values (RLUmax) were calculated by GraphPad Prism 7.0 version.

Binding Affinity Assay. The binding affinity of compounds with the human PD-L1 IgV domain (human PD-L1/B7-H1 protein, His tag, PD-1-H5229) and the human PD-1 IgV domain (human PD-1/PDCD1 protein, Fc tag, ACRO, PD-1-H5257) was examined on a Biacore T200 (GE Healthcare Biosciences, Sweden). Briefly, His-PD-L1 or Fc-PD-1 was diluted using 1× phosphate-buffered saline (PBST) buffer (99.95% PBS + 0.05% Tween 20) and immobilized onto one CM5 chip, all in 10 mM sodium acetate (pH 4.5) by a standard amine-coupling procedure. Compounds were serially diluted with the phosphate-buffered saline (PBS) buffer containing 0.05% Tween 20 and 5% DMSO to appropriate concentrations and injected at a flow through the chip following the preset program. The K_D value was determined with Biacore T200 evaluation software (GE Healthcare).

Pharmacokinetic Study. The pharmacokinetic studies on selected compounds were conducted by Medicilon (Shanghai, China). Briefly, male Sprague−Dawley rats or C57BL/6 mice were prohibited diet 12 h before the experiment. Blood samples (0.2 mL) were collected from the jugular vein at 0.0833, 0.25, 0.5, 1, 1.5, 2, 4, 8, 12, and 24 h after oral or intravenous administration. The data was detected by liquid chromatography−mass spectrometry (LC−MS; TQ6500+ Triple quad), and PK parameters were determined by Phoenix WinNonlin7.0.

B16-F10 Melanoma Mouse Model. All animal studies were conducted in accordance with the guiding principles of the Animal Care and Use Committee of the China Pharmaceutical University (Nanjing, China).

C57BL/6J mice (female, 8 week old) were purchased from Beijing Vital River Laboratory Animal Technology (Beijing, China) and maintained under a controlled environment at 25 °C for a 12 h light/dark cycle, with free access to food and water. B16-F10 tumors were established by injecting 1 × 10^6 B16-F10 cells in PBS into the dorsal area of mice. The mice bearing tumors were randomly divided into four groups and treated with 0.5% sodium carboxymethyl cellulose (CMC-Na) (vehicle), **L24** (15 mg/kg), **L24** (45 mg/kg), and CTX (80 mg/kg) by oral gavage daily. Treatment started on the same day when the tumor cells were injected (day 1). Tumor dimensions and animal body weights were measured every day. Tumor volumes were calculated according to the following formula: volume (mm^3) = 0.5 × length (mm) × width (mm) × width (mm). On day 18, the mice were sacrificed and the tumors were isolated. Tumor growth inhibition (TGI) rates were calculated using the following formula: TGI (%) = $[1 - V_t/V_v] \times 100\%$, where V_t and V_v are the mean tumor volumes of the treatment group and vehicle control, respectively.

MC38 Tumor Mouse Model. C57BL/6J mice (female, 8 week old) were purchased from Beijing Vital River Laboratory Animal Technology (Beijing, China) and maintained under a controlled environment at 25 °C in a 12 h light/dark cycle, with free access to food and water. MC38 tumors were established by injecting 1 × 10^6 MC38 cells in PBS into the dorsal area of mice. When the tumor volume reached 50 mm^3, the mice bearing tumors were randomly divided into four groups and treated with CMC-Na (vehicle), **L24** (50 mg/kg), **L24** (150 mg/kg), and **L24** (300 mg/kg) by oral gavage daily. Tumor dimensions and animal body weights were measured every two days. Tumor volumes were calculated according to the following formula: volume (mm^3) = 0.5 × length (mm) × width (mm) × width (mm). After 18 days of treatment, the mice were sacrificed and the tumors were isolated. Tumor growth inhibition (TGI) rates were calculated as mentioned above.

PD-L1 Humanized Tumor Mouse Model. The PD-L1 humanized C57BL/6 mice (female, 6 week old) and MC38-hPD-L1(Tg)-mPDL1(KO) cells were purchased from GemPharmatech (Nanjing, China). PD-L1-humanized C57BL/6 mice were injected with 1 × 10^6 MC38-hPD-L1(Tg)-mPDL1(KO) cells in PBS into the right flank area. When the tumor volume reached 50 mm^3, the mice bearing tumors were randomly divided into three groups and treated with CMC-Na (vehicle) and **L24** (5 and 25 mg/kg) by oral gavage daily. Tumor dimensions and animal body weights were measured twice a week. Tumor volumes were calculated according to the following formula: volume (mm^3) = 0.5 × length (mm) × width (mm) × width (mm). On day 27, the mice were sacrificed and the tumors were isolated. Tumor growth inhibition (TGI) rates were calculated as mentioned above.

Flow Cytometry. Antibodies were purchased from BD Biosciences, eBioscience, or Invitrogen. The tumor tissue was isolated and digested into a single-cell suspension. Red blood cells were lysed by ACK lysis buffer and incubated with Fc block antibodies. For cell surface staining, the cells were incubated with antibodies anti-CD45 (BV510), anti-CD3 (BV711), anti-CD4 (APC-H7), anti-CD8 (PE), anti-CD335 (AF647), anti-CD11b (PE-CF594), anti-Ly6G (BV421), anti-Ly6C (FITC), anti-F4/80 (Super Bright 600) for 60 min, and after washing twice with PBS, sytoxAAD (Invitrogen, S10274) was added before being read on flow cytometry. As for intracellular staining, cells were labeled with FVS780 (BD, 565388), permeabilized with Transcription Factor Staining Buffer (eBioscience, 00-5523) after surface staining, and incubated with anti-FOXP3 (PE) for 60 min. All samples were read on an Attune NxT (Thermo).

■ ASSOCIATED CONTENT

Supporting Information

The Supporting Information is available free of charge at https://pubs.acs.org/doi/10.1021/acs.jmedchem.1c00392.

https://doi.org/10.1021/acs.jmedchem.1c00392
J. Med. Chem. 2021, 64, 8391−8409

^{1}H NMR, ^{13}C NMR, and UPLC spectra of target compounds; figures of pharmacokinetic studies; toxicity data *in vivo* and *in vitro* (PDF)

Docking models (5J89-BMS-1016-XP) (PDB)

Docking models (5J89-L1-XP) (PDB)

Docking models (5J89-L7-XP-refine) (PDB)

Molecular formula strings (CSV)

AUTHOR INFORMATION

Corresponding Authors

Haoliang Yuan − *Jiangsu Key Laboratory of Drug Discovery for Metabolic Disease, State Key Laboratory of Natural Medicines, China Pharmaceutical University, Nanjing 210009, China;* orcid.org/0000-0003-0248-4347; Email: yhl@cpu.edu.cn

Hongbin Sun − *Jiangsu Key Laboratory of Drug Discovery for Metabolic Disease, State Key Laboratory of Natural Medicines, China Pharmaceutical University, Nanjing 210009, China; State Key Laboratory for the Chemistry and Molecular Engineering of Medicinal Resources, School of Chemistry and Pharmacy, Guangxi Normal University, Guilin 541004, China;* orcid.org/0000-0002-3452-7674; Phone: +86-25-83271196; Email: hongbinsun@cpu.edu.cn

Authors

Liu Liu − *Jiangsu Key Laboratory of Drug Discovery for Metabolic Disease, State Key Laboratory of Natural Medicines, China Pharmaceutical University, Nanjing 210009, China*

Zhiying Yao − *Jiangsu Key Laboratory of Drug Discovery for Metabolic Disease, State Key Laboratory of Natural Medicines, China Pharmaceutical University, Nanjing 210009, China*

Shijun Wang − *Jiangsu Key Laboratory of Drug Discovery for Metabolic Disease, State Key Laboratory of Natural Medicines, China Pharmaceutical University, Nanjing 210009, China*

Tao Xie − *Jiangsu Key Laboratory of Drug Discovery for Metabolic Disease, State Key Laboratory of Natural Medicines, China Pharmaceutical University, Nanjing 210009, China*

Guoqing Wu − *Jiangsu Key Laboratory of Drug Discovery for Metabolic Disease, State Key Laboratory of Natural Medicines, China Pharmaceutical University, Nanjing 210009, China*

Honghan Zhang − *Jiangsu Key Laboratory of Drug Discovery for Metabolic Disease, State Key Laboratory of Natural Medicines, China Pharmaceutical University, Nanjing 210009, China*

Pu Zhang − *Jiangsu Flag Chemical Industry Co., Ltd., Nanjing 211500, China*

Yaojun Wu − *Jiangsu Flag Chemical Industry Co., Ltd., Nanjing 211500, China*

Complete contact information is available at: https://pubs.acs.org/10.1021/acs.jmedchem.1c00392

Author Contributions

$^{\|}$L.L., Z.Y., and S.W. contributed equally to this work.

Notes

The authors declare no competing financial interest.

ACKNOWLEDGMENTS

Financial support from the Jiangsu Natural Science Foundation (BK20202009) is gratefully acknowledged. This research was also supported by the National Natural Science Foundation of China (81730094, 81773584, and 21977118).

ABBREVIATIONS

PD-1, programmed cell death-1; PD-L1, programmed cell death-ligand 1; HTRF, homogeneous time-resolved fluorescence; SPR, surface plasmon resonance; mAbs, monoclonal antibodies; FDA, Food and Drug Administration; irAEs, immune-related adverse effects; VISTA, V-domain Ig suppressor of T-cell activation; DMF, *N*,*N*-dimethylformamide; DIPEA, *N*,*N*-diisopropylethylamine; Pd(dppf)Cl_2.CH_2Cl_2, [1,1′-bis(diphenylphosphino) ferrocene] dichloropalladium (II), complex with dichloromethane; NFAT, nuclear factor of activated T cells; TCR, T-cell receptor; PK, pharmacokinetic; AST, aspartate aminotransferase; ALT, alanine aminotransferase; CK, creatine kinase; BUN, blood urea nitrogen; TGI, tumor growth inhibition; CTX, cyclophosphamide; MDSC, myeloid-derived suppressor cell; MΦs, macrophages; NK cells, natural killer cells; TAMs, tumor-associated macrophages; TILs, tumor-infiltrating lymphocytes

REFERENCES

(1) Ribas, A.; Wolchok, J. D. Cancer immunotherapy using checkpoint blockade. *Science* **2018**, *359*, 1350−1355.

(2) Sharma, P.; Allison, J. P. The future of immune checkpoint therapy. *Science* **2015**, *348*, 56−61.

(3) Chen, Y.; Pei, Y.; Luo, J.; Huang, Z.; Yu, J.; Meng, X. Looking for the optimal PD-1/PD-L1 inhibitor in cancer treatment: a comparison in basic structure, function, and clinical practice. *Front. Immunol.* **2020**, *11*, No. 1088.

(4) Hodi, F. S.; O'Day, S. J.; McDermott, D. F.; Weber, R. W.; Sosman, J. A.; Haanen, J. B.; Gonzalez, R.; Robert, C.; Schadendorf, D.; Hassel, J. C.; Akerley, W.; van den Eertwegh, A. J. M.; Lutzky, J.; Lorigan, P.; Vaubel, J. M.; Linette, G. P.; Hogg, D.; Ottensmeier, C. H.; Lebbé, C.; Peschel, C.; Quirt, I.; Clark, J. I.; Wolchok, J. D.; Weber, J. S.; Tian, J.; Yellin, M. J.; Nichol, G. M.; Hoos, A.; Urba, W. J. Improved survival with ipilimumab in patients with metastatic melanoma. *N. Engl. J. Med.* **2010**, *363*, 711−723.

(5) Boussiotis, V. A. Molecular and biochemical aspects of the PD-1 checkpoint pathway. *N. Engl. J. Med.* **2016**, *375*, 1767−1778.

(6) Finn, R. S.; Qin, S.; Ikeda, M.; Galle, P. R.; Ducreux, M.; Kim, T. Y.; Kudo, M.; Breder, V.; Merle, P.; Kaseb, A. O.; Li, D.; Verret, W.; Xu, D. Z.; Hernandez, S.; Liu, J.; Huang, C.; Mulla, S.; Wang, Y.; Lim, H. Y.; Zhu, A. X.; Cheng, A. L.; Investigators, I.M.. Atezolizumab plus bevacizumab in unresectable hepatocellular carcinoma. *N. Engl. J. Med.* **2020**, *382*, 1894−1905.

(7) Hack, S. P.; Zhu, A. X.; Wang, Y. Augmenting anticancer immunity through combined targeting of angiogenic and PD-1/PD-L1 pathways: Challenges and opportunities. *Front. Immunol.* **2020**, *11*, No. 598877.

(8) Yang, J.; Hu, L. Immunomodulators targeting the PD-1/PD-L1 protein-protein interaction: from antibodies to small molecules. *Med. Res. Rev.* **2019**, *39*, 265−301.

(9) Kamada, T.; Togashi, Y.; Tay, C.; Ha, D.; Sasaki, A.; Nakamura, Y.; Sato, E.; Fukuoka, S.; Tada, Y.; Tanaka, A.; Morikawa, H.; Kawazoe, A.; Kinoshita, T.; Shitara, K.; Sakaguchi, S.; Nishikawa, H. PD-1(+) regulatory T cells amplified by PD-1 blockade promote hyperprogression of cancer. *Proc. Natl. Acad. Sci. U.S.A.* **2019**, *116*, 9999−10008.

(10) Bailly, C.; Vergoten, G. Protein homodimer sequestration with small molecules: Focus on PD-L1. *Biochem. Pharmacol.* **2020**, *174*, No. 113821.

(11) Zak, K. M.; Grudnik, P.; Magiera, K.; Domling, A.; Dubin, G.; Holak, T. A. Structural biology of the immune checkpoint receptor PD-1 and its ligands PD-L1/PD-L2. *Structure* **2017**, *25*, 1163−1174.
(12) Zak, K. M.; Kitel, R.; Przetocka, S.; Golik, P.; Guzik, K.; Musielak, B.; Domling, A.; Dubin, G.; Holak, T. A. Structure of the complex of human programmed death 1, PD-1, and its ligand PD-L1. *Structure* **2015**, *23*, 2341−2348.
(13) Chen, Y.; Liu, P.; Gao, F.; Cheng, H.; Qi, J.; Gao, G. F. A dimeric structure of PD-L1: functional units or evolutionary relics? *Protein Cell* **2010**, *1*, 153−160.
(14) Li, K.; Tian, H. Development of small-molecule immune checkpoint inhibitors of PD-1/PD-L1 as a new therapeutic strategy for tumour immunotherapy. *J. Drug Targeting* **2019**, *27*, 244−256.
(15) Wang, T.; Wu, X.; Guo, C.; Zhang, K.; Xu, J.; Li, Z.; Jiang, S. Development of inhibitors of the programmed cell death-1/programmed cell death-ligand 1 signaling pathway. *J. Med. Chem.* **2019**, *62*, 1715−1730.
(16) Cheng, B.; Ren, Y.; Niu, X.; Wang, W.; Wang, S.; Tu, Y.; Liu, S.; Wang, J.; Yang, D.; Liao, G.; Chen, J. Discovery of novel resorcinol dibenzyl ethers targeting the programmed cell death-1/programmed cell death-ligand 1 interaction as potential anticancer agents. *J. Med. Chem.* **2020**, *63*, 8338−8358.
(17) Qin, M.; Cao, Q.; Zheng, S.; Tian, Y.; Zhang, H.; Xie, J.; Xie, H.; Liu, Y.; Zhao, Y.; Gong, P. Discovery of [1,2,4]Triazolo[4,3-a]pyridines as potent inhibitors targeting the programmed cell death-1/programmed cell death-ligand 1 interaction. *J. Med. Chem.* **2019**, *62*, 4703−4715.
(18) Chupak, L. S.; Zheng, X. Compounds Useful as Immunomodulators. Bristol-Myers Squibb Co., WO2015034820, 2015.
(19) Chupak, L. S.; Ding, M.; Martin, S. W.; Zheng, X.; Hewawasam, P.; Connoly, T. P.; Xu, N.; Yeung, K.-S.; Zhu, J.; Langley, D. R.; Tenney, D. J.; Scola, P.M. Compounds useful as immunomodulators. Bristol-Myers Squibb Co., WO2015160641, 2015.
(20) Zak, K. M.; Grudnik, P.; Guzik, K.; Zieba, B. J.; Musielak, B.; Dömling, A.; Dubin, G.; Holak, T. A. Structural basis for small molecule targeting of the programmed death ligand 1 (PD-L1). *Oncotarget* **2016**, *7*, 30323−30335.
(21) Ganesan, A.; Ahmed, M.; Okoye, I.; Arutyunova, E.; Babu, D.; Turnbull, W. L.; Kundu, J. K.; Shields, J.; Agopsowicz, K. C.; Xu, L.; Tabana, Y.; Srivastava, N.; Zhang, G.; Moon, T. C.; Belovodskiy, A.; Hena, M.; Kandadai, A. S.; Hosseini, S. N.; Hitt, M.; Walker, J.; Smylie, M.; West, F. G.; Siraki, A. G.; Lemieux, M. J.; Elahi, S.; Nieman, J. A.; Tyrrell, D. L.; Houghton, M.; Barakat, K. Comprehensive in vitro characterization of PD-L1 small molecule inhibitors. *Sci. Rep.* **2019**, *9*, No. 12392.
(22) Lee, H. T.; Lee, J. Y.; Lim, H.; Lee, S. H.; Moon, Y. J.; Pyo, H. J.; Ryu, S. E.; Shin, W.; Heo, Y. S. Molecular mechanism of PD-1/PD-L1 blockade via anti-PD-L1 antibodies atezolizumab and durvalumab. *Sci. Rep.* **2017**, *7*, 5532.
(23) Inman, B. A.; Longo, T. A.; Ramalingam, S.; Harrison, M. R. Atezolizumab: a PD-L1-blocking antibody for bladder cancer. *Clin. Cancer Res.* **2017**, *23*, 1886−1890.
(24) Lin, D. Y- W.; Tanaka, Y.; Iwasaki, M.; Gittis, A. G.; Su, H. P.; Mikami, B.; Okazaki, T.; Honjo, T.; Minato, N.; Garboczi, D. N. The PD-1/PD-L1 complex resembles the antigen-binding Fv domains of antibodies and T cell receptors. *Proc. Natl. Acad. Sci. U.S.A.* **2008**, *105*, 3011−3016.
(25) De La Rochere, P.; Guil-Luna, S.; Decaudin, D.; Azar, G.; Sidhu, S. S.; Piaggio, E. Humanized mice for the study of immuno-oncology. *Trends Immunol.* **2018**, *39*, 748−763.
(26) Long, E. O.; Kim, H. S.; Liu, D.; Peterson, M. E.; Rajagopalan, S. Controlling natural killer cell responses: integration of signals for activation and inhibition. *Annu. Rev. Immunol.* **2013**, *31*, 227−258.
(27) Tumeh, P. C.; Harview, C. L.; Yearley, J. H.; Shintaku, I. P.; Taylor, E. J.; Robert, L.; Chmielowski, B.; Spasic, M.; Henry, G.; Ciobanu, V.; West, A. N.; Carmona, M.; Kivork, C.; Seja, E.; Cherry, G.; Gutierrez, A. J.; Grogan, T. R.; Mateus, C.; Tomasic, G.; Glaspy, J. A.; Emerson, R. O.; Robins, H.; Pierce, R. H.; Elashoff, D. A.; Robert, C.; Ribas, A. PD-1 blockade induces responses by inhibiting adaptive immune resistance. *Nature* **2014**, *515*, 568−571.
(28) Qian, B. Z.; Pollard, J. W. Macrophage diversity enhances tumor progression and metastasis. *Cell* **2010**, *141*, 39−51.
(29) Noman, M. Z.; Desantis, G.; Janji, B.; Hasmim, M.; Karray, S.; Dessen, P.; Bronte, V.; Chouaib, S. PD-L1 is a novel direct target of HIF-1alpha, and its blockade under hypoxia enhanced MDSC-mediated T cell activation. *J. Exp. Med.* **2014**, *211*, 781−790.
(30) Kontoyianni, M.; McClellan, L. M.; Sokol, G. S. Evaluation of docking performance: comparative data on docking algorithms. *J. Med. Chem.* **2004**, *47*, 558−565.

https://doi.org/10.1021/acs.jmedchem.1c00392
J. Med. Chem. 2021, 64, 8391−8409